Title: Large quantities of small microplastics permeate the surface ocean to abyssal depths in the South Atlantic Gyre

Running title: Microplastics in the ocean's interior

Authors

Shiye Zhao,[1,2]* Erik R. Zettler,[3] Ryan P. Bos,[1] Peigen Lin,[4] Linda A. Amaral-Zettler,[3,5,6] Tracy J. Mincer,[1,7]*

Affiliations

[1]Harbor Branch Oceanographic Institute, Florida Atlantic University, Fort Pierce, FL 34946, USA

[2]Japan Agency for Marine-Earth Science and Technology, 2-15 Natsushimacho, Yokosuka 237-0061, Japan

[3]Department of Marine Microbiology and Biogeochemistry, NIOZ Royal Netherlands Institute for Sea Research, Den Burg, Texel, The Netherlands

[4]Woods Hole Oceanographic Institution, Woods Hole MA, USA

[5]Department of Freshwater and Marine Ecology, Institute for Biodiversity and Ecosystem Dynamics, University of Amsterdam, Amsterdam, The Netherlands

[6]The Josephine Bay Paul Center for Comparative Molecular Biology and Evolution, Marine Biological Laboratory, Woods Hole, MA, USA

[7]Department of Biology, Wilkes Honors College, Florida Atlantic University, Jupiter, FL 33458, USA

*Corresponding authors: szhao@jamstec.go.jp, tmincer@fau.edu

Abstract

Hundreds of studies have surveyed plastic debris in surface ocean gyre and convergence zones, however, comprehensive microplastics (MP, ≤5 mm) assessments beneath these surface accumulation areas are lacking. Using *in-situ* high-volume filtration, Manta net and MultiNet sampling, combined with micro-Fourier-transform-infrared imaging, we discovered a high abundance (up to 244.3 pieces per cubic meter [n m^{-3}]) of small microplastics (SMP, characteristically <100 μm) from the surface to near-sea floor waters of the remote South Atlantic Subtropical Gyre. Large horizontal and vertical variations in the abundances of SMP were observed, displaying inverse vertical trends in some cases. SMP abundances in pump samples were over 2 orders of magnitude higher than large microplastics (LMP, >300 μm) concurrently collected in MultiNet samples. Higher density polymers (e.g., alkyd resins and polyamide) comprised >65% of the total pump sample count, highlighting a discrepancy between polymer compositions from previous ocean surface-based surveys, typically dominated by buoyant polymers such as polyethylene and polypropylene. Contrary to previous reports stating LMP preferentially accumulated at density gradients, SMP with presumably slower sinking rates are much less influenced by density gradients, thus resulting in a more even vertical distribution in the water column, and potentially longer residence times. Overall, our findings suggest that SMP is a critical and largely underexplored constituent of the oceanic plastic inventory. Additionally, our data support that weak current systems contribute to the formation of SMP hotspots at depth, implying a higher encounter rate for subsurface particle feeders. Our study unveils the prevalence of plastics in the entire water column, highlighting the urgency for more quantification of the deep-ocean MP, particularly the smaller size fraction, to better understand ecosystem exposure and to predict MP fate and impacts.

Key words: FTIR imaging, *in-situ* pump, microplastics, plastic marine debris, South Atlantic Gyre, water column

Introduction

It has been estimated that between 19 and 23 million metric tons of plastic waste entered the world's aquatic ecosystems in 2016 alone (*1*). Much of this plastic waste ultimately enters the marine environment, where it is fragmented via physical, chemical and biological processes (*2*), and subsequently a portion of these plastics are transported across the World Ocean. Currently, up to 51 trillion microplastic (MP) particles are estimated to be floating in the surface waters of the global ocean (*3*). However, a size-selective loss of MP has been observed at the sea surface (*4, 5*), suggesting the surface ocean is not the ultimate sink for plastic debris, bringing the ultimate fate of MP into question. Empirical evidence and modelling studies suggest that biological and physical processes of the upper ocean could redistribute MP drifting at sea throughout the pelagic water column (*6*). A vast majority of plastic marine debris surveys, however, have focused on surface waters (*4, 5, 7*), and to a lesser extent, deep-sea sediments (*8-10*).

Although the deep sea is Earth's largest ecosystem by volume and area (*11*), waters below 200 m (*12*) are just beginning to be explored for MP distributions and include the following: a report by La Daana et al. (*13*) showed that MP depth profiles ranged from 0-375 n m^{-3} in the Arctic Central Basin, which were analyzed and reported from Niskin bottles collected water samples (7-12 L); a study by Choy et al. (*14*) employed a large volume (1007-2378 m^3 per sample) *in-situ* filtration technique to harvest across epi- and mesopelagic depths to quantify MP abundances (~1.0-15.0 n m^{-3}) in Monterey Bay; and a study by Ross et al. found average MP was 37.3 n m^{-3} in Niskin-bottle collected seawater samples (29-67 L) and determined these plastics to be pervasive throughout the water column in the Beaufort Sea (*15*). Nevertheless, all of these studies were limited to spectroscopic measurements that relied on visual presorting of plastic-like particles and inherently could not reliably include MP <100 μm, a fraction previously demonstrated by other

workers to be numerically abundant in the ocean (*16, 17*). Using micro-Fourier transform infrared (μFTIR) spectroscopic imaging with automated data analysis, Tekman et al. (*18*) measured MP concentrations from surface waters to deep-sea sediments by filtering >200 L of seawater in the Arctic. The authors unveiled typical concentrations spanning 0-1287 n m^{-3}, with MP ≤25 μm accounting for more than 50% of the particle counts in each sample.

As plastic particles disintegrate into smaller size fractions, they can become harmful in different and unpredictable ways that are only beginning to be understood. For example, MP smaller than 150 μm can translocate across the gut epithelium (*19*), become trapped in biomass, and have the potential to transfer through marine food webs, posing an unknown ecological risk and biogeochemical impacts. The occurrence of these smaller MP in food webs and surrounding seawaters, however, is underreported due to the difficulty of sampling high volumes of water and the need for specialized analytical methods required for characterizing small particles from samples (*20*).

The presence of accumulation zones of plastic marine debris located within the five subtropical gyres has been verified (*4, 5, 7*). These studies all focused on LMP collected via surface-trawl plankton nets and were sorted visually. To date, only two studies have reported the presence of smaller MP (<300 μm) in the surface waters of the North Atlantic Gyre (*16, 21*). Most recently, 11.6-21.1 million tonnes of polyethylene (PE), polypropylene (PP), and polystyrene (PS) MP (32-651 μm) were estimated to be in the top 200 m of the Atlantic Ocean after collection from three discrete depths along a north-south transect with in-situ pumps and μFTIR polymer identification (*22*); however, this study was limited to only PE, PP and PS, presenting a possible knowledge gap of other plastic polymers (*22*). Recently, other polymers (e.g., polyamide, polyurethane) rather than PE, PP and PS have been reported to be the dominant plastics of sub-surface marine samples

(*18, 23*). Therefore, a more complete dataset containing all identified polymers is necessary to provide a comprehensive understanding of ocean plastic pollution. It is plausible that small MP are ubiquitous in the deep-ocean waters underneath offshore plastic accumulation zones, based on their high abundances in the upper layer (<200 m) of mid-latitude oceanic gyres mentioned above (*16, 21, 22*). Furthermore, the observations of open-ocean SMP in the shallow and deep-pelagic waters have only been reported in two studies (*18, 22*), both of which disclosed the inconsistency of the vertical trends of plastic abundance and distribution across sampling stations. This unclear pattern in vertical profiles of water-column plastics has been attributed to the unknown redistribution and removal processes in the ocean interior (*6*). A better mechanistic understanding of how plastics sink from the ocean surface beyond the mixed layer and ultimately to abyssal depths is critical to predicting its fate and impacts on the marine ecosystems.

In this study we sampled plastic particles in the South Atlantic Subtropical Gyre (SASG, Fig. 1) by deploying a combination of surface Manta nets (*SI Appendix*, Table S1), multiple opening/closing nets at discrete depths in the top 100 m (*SI Appendix*, Table S1), and McLane *in-situ* Large Volume Water Transfer System (WTS-LV) pumps at four different stations from surface to near-seafloor depths (*SI Appendix*, Table S2) in the South Atlantic plastic accumulation zone (*4*). Our combined analysis procedure, including the automated interpretation of spectral datasets created by µFTIR imaging, provide a more integrative view of the distribution, abundance, dimensions and chemical nature of plastic particles in the interior of an ocean gyre.

Methods

***Study Area and Sample Collection*.** Samples were collected while onboard the RV *Pelagia* cruise 64PE-448 during the 21-day long "Sinergia" SASG Cruise (January 4th-24th, 2019). Two stations (A, D) located in the outer accumulation zone of the SASG, and two stations (B, C) located in the inner accumulation zone, were chosen to collect oceanic particle samples in the water column

(Fig.1). According to previous model results (*4*, *5*), the outer accumulation zone of the SASG has a modeled average concentration of surface plastics of ~100 g per km^2, while the inner accumulation zone shows a mean concentration of plastics of ~600 g per km^2. Manta net (Oceaninstruments) and MultiNet (Hydro-bios) samples (Fig.1 and S1, Table S1) were collected before deploying the WTS-LV pumps (LV08, McLane Research Laboratories). Four WTS-LV pumps were used in total: three pumps were fitted with three standard radial filter holders and one pump was fitted with a 3-tier filter holder. All filter holders were made of black acetal which we analyzed for our polymer workflow library. The site of deploying the WTS-LV pumps at each station were purposely distant (on average about 5 nautical miles) from the location where the Manta net and MultiNet were retrieved. These intervals assured the prevention of potential contamination of pump samples from the possible shedding of nylon fiber from the mesh material of the Manta net and MultiNet collection devices. For the details of net and pump samplings, please refer to Table S1 and S2. Manta trawls were carried out using a Manta net (0.86 m wide × 0.15 m vertical opening) with a 500 µm mesh net and a closed cod end. The MultiNet had an opening of 0.5 × 0.5 m, with 200 µm mesh nets and plastic cod ends with 100 µm mesh windows. The Manta nets were towed in a straight line for 30 minutes at 2 knots at each Manta net tow station (n = 5, MT-05, -14, -16, -18, -22, Fig.1). The MultiNet samples were collected at five different depths (Table S1). The net was lowered to the maximum depth with all nets closed, then nets were opened/closed individually and towed for 25-48 min at each depth. The net depth was monitored continuously and maintained within 3 m of the target depth, then closed before raising the frame to the next depth. Three MultiNet deployments (MN-01 at depths of 20, 40, 60, 80 100 m; both MN-02 and MN-03 at depths of 5, 10, 20, 40, 60 m) were conducted around the WTS-LV pump stations A, B and C (Fig.1, Table S1 and S2). The volume of seawater filtered was determined from the readings of a mechanic flowmeter (2030RC, General Oceanics) within the mouth of the net. Once the net (Manta net or MultiNet) was retrieved from the sea, it was

thoroughly rinsed on board with a seawater hose from the outside inwards, from the mouth toward the end to accumulate all the material in the cod-end. Then, the cod-end was removed and rinsed down into a clean bucket. In the onboard laboratory, any plastic-like particles floating in each bucket were picked out visually. Then remaining samples in the bucket were poured onto a 300-µm mesh size sieve. Once sieved, the content retained was carefully examined, and plastic-like particles were transferred to the white plastic tray. When in doubt, the particle was checked with the aid of a stereomicroscope and retained for FTIR analysis. Counts were documented for each Manta net and MultiNet sample. Finally, particles were dried and stored in the dark in glass scintillation vials with foil lined caps (20 ml) for polymer analysis (see below).

At each station, a conductivity-temperature depth (CTD, Sea-Bird Electronics) profile was collected to measure standard parameters (e.g., conductivity, temperature, dissolved oxygen) of the deployment area. Using the profiles of these parameters (Fig. S2), distinct water layers of interest were identified such as the mixed layer, pycnocline, Antarctic Intermediate Water (AAIW) and the Antarctic Bottom Water (AABW). The WTS-LV pumps were tethered to a single wire and deployed at predetermined depths (Fig.S2, Table S2) using a modified pumping method (*24*). For each pump unit, seawater was directed through a series of filters: The samples passed through stacked pre-combusted 200 and 40 µm stainless steel (SS) mesh screens followed by the pre-combusted 2.0 µm quartz fiber filter (Whatman QM-A). Thus, >200, 40-200, and 2-40 µm size-fraction particles were retained by the SS and QM-A filters. The effective filtration area of these filters was ~125 cm^2. The reasons for selecting QM-A filters were as follows: 1) quartz fiber filters can be pre-combusted to avoid potential contamination, which is particularly important for studying small microplastic; and, 2) in comparison to membrane filters, QM-A filters have better particle loading and uniformity (*24*). The disadvantage of using QM-A filters, however, is that its pore tortuosity (a fluid dynamic term for the complex path a particle takes

with twists and turns) is better suited for trapping particles at the surface and inside the filter media. However, retaining particles within the filter layers is not conducive to particle extraction and thus probably results in an underestimation of plastic abundances. During particle extraction in this study disintegration of QM-A filters was observed which would release the entrapped particles and improve recovery rate.

All pumps were programmed to run for five hours and stop if flow rates fell below 3-4 L/minute, resulting in a range of 440 to 1765 L seawater filtered, depending on *in-situ* particle concentrations (Table S2). Of all filters, only QM-A filters, which collected 2-40 µm sized particles, were analyzed in this study. The QM-A filters and SS meshes were folded and wrapped with pre-combusted foil, and immediately stored at -80 ^{o}C until analysis. At the end of the cruise, all filters were transported on dry ice to the laboratory and stored at -80 ^{o}C prior to further processing. Calm seas prevailed during the WTS-LV pump sampling (Table S1).

***Extraction of SMP* in Pump Samples.** To isolate SMP, the QMA filters wrapped within the aluminum foil were thawed to room temperature for ~3 h under a laminar flow hood. Three subsamples of the QM-A filters from each pump were taken with a flamed metal punch (23 mm diam.) sampling along the surface. Based on the filtration efficiency and filtration area calculations of the QM-A filters, each subsample corresponded to ~100 L of filtered seawater and were therefore recognized as one technical replicate. A total of three technical replicates were analyzed for each pump, and the filtered seawater volume of each replicate ranged from 102.3 L to 139.9 L (Table S1). For each replicate, the sub-sampled QM-A filters were placed into separate pre-combusted borosilicate glass scintillation vials (20 ml, DMK, Life Sciences Kimble) containing sodium iodide (NaI: 1.65-1.70 g cm^{-3}) and sonicated for 5 min. These subsamples were then pooled into a 50 ml conical centrifugation tube (DMK, Life Sciences Kimble) and

centrifuged at 1600 rpm for 15 minutes. The supernatant was filtered onto a pre-combusted stainless-steel filter (5 µm), and this procedure was repeated at least three times per replicate. The sample on the stainless-steel filter was stored in a scintillation vial with 5 ml 5% potassium hydroxide at 60 °C for 24 hours for removal of organic matter. Potassium hydroxide was neutralized with hydrochloric acid, and particles on the stainless-steel filter were detached by sonication for 5 minutes. Particles in the liquid were concentrated onto an Anodisc filter (0.2 µm pore size, GE Whatman) held in a glass filter holder (Advantec, 13 mm in diameter), followed by a thorough vial rinsing step with 50% ethanol to remove SMP that could possibly adhere to the glass vessel. The rinsing steps was done three times to increase SMP yields. The Anodisc filter was then dried at 37 °C overnight prior to µFTIR analyses.

To test the influences of the sample storage and experimental steps, aged plastics (n=10) from our Manta net samples were placed into a pre-combusted glass scintillation vial and stored at -80 °C for 3 days. Plastics were subsequently thawed at room temperature for 3 hours and processed following the identical procedure as the samples. The mechanical transformation was evaluated by comparing the geometries (i.e., Feret diameter) and weights of these particles at pre-test to post-test. No apparent changes were found.

Polymer Analysis. SMP particles were identified by µFTIR spectroscopy (Thermo Scientific™ Nicolet™ iN10, USA) in a HEPA filtered laminar flow hood. The entire sample-filter area (13 mm in diameter) was mapped using the FTIR microscope in transmission mode using an MCT/A detector (aperture size: 25 µm × 25 µm, 1 scan at 16 cm^{-1} resolution, step size: 21 and 22 µm). The background position was selected as an area clear of particles on the Anodisc filter. Upon acquiring the FTIR chemical images of samples (more than 17 million individual spectra were generated in total), the particle polymer types were confirmed using two steps (Fig. S3): (Step I)

All spectra of the resulting chemical maps were subject to preprocessing with the auto-baseline correction and normalization in OMNIC Picta (Thermo Fisher Scientific, USA). All spectra within the whole chemical map were exported to CSV files and SPA files. Then all the spectra (CSV files) were compared automatically against a transformed reference library (*25*) with the search algorithm (Pearson's correlation) using a Python script. When Pearson's correlation coefficient between the experimental and the library spectrum was larger than 0.8, the position and polymer types of each identified spectrum were recorded; (Step II) Based on the coordinates, spectra were tracked in chemical maps, and the polymer identity was confirmed by comparing with the Hummel Polymer Sample Library in OMNIC Picta. The software interpretation was systematically validated (>70% match with reference spectra) or rejected (<60% match with reference spectra). Spectra with a match between 60% and 70% were individually reinterpreted by confirming the clear presence of specific polymer peaks. The particle was only verified to be plastic if its spectrum was confirmed as the same polymer type by both steps. Procedure blanks were scanned and analyzed with the same methods.

To verify the polymer composition in the Manta net samples, the FTIR Spectrometer (Thermo Scientific™ Nicolet™ iN10, USA) in the attenuated total reflection mode in the spectral range from 3600 to 1250 cm^{-1} was applied to selected particles. A total of 33% (n = 457) of the total particles collected in nets (n = 1406) was analyzed. The polymer type of each particle was confirmed by comparing its FTIR spectra against the Hummel Polymer Sample Library in OMNIC Picta. The polymer composition was identified according to the criteria mentioned above.

***Oxidation Degree*.** Plastics are manufactured with different additives (e.g., plasticizers, stabilizers) based on polymer application (e.g., plasticizers, stabilizers) and therefore may differ

in their reaction to various levels of environmental exposure to temperature and ultraviolet light. Consequently, plastic debris may exhibit a large variety of degradation signatures. Characterizing weathering degree is critical to better understand the origin and fate of environmental plastics (*15*). The carbonyl indices have been often used to estimate the weathering degree of plastics in literature (*15, 26, 27*). Therefore, PE polymers, the most common resin types found in the open ocean, were selected to study oxidation degree by comparing carbonyl indices. The carbonyl indices of PE large microplastics (PE-LMP) in the Manta net samples and the PE small microplastics (PE-SMP) collected by the WTS-LV pumps were calculated by measuring the ratio of the absorbance band area of the carbonyl group at 1630-1850 cm^{-1} and the olefinic band area at 1420-1490 cm^{-1} (*28, 29*). Although little degradation of plastics due to the 10% KOH processing step has been documented (*30-32*) we took the extra precaution in our study to employ 5% KOH to purify samples and calculated carbonyl index based on two band areas, which differs from previously published methods (two spectral peaks), thus further minimizing the potential artifacts of KOH treatment on FTIR spectra and carbonyl index determination.

***SMP Characteristics*.** The optical images of particles were often partially blurred due to the combination of irregularly shaped particles and the motion of particles during the high-speed imaging (10 steps per second). Therefore, the major (the maximum Ferret's diameter) and the minor axes (the longest axis perpendicular to the major axis) of each SMP were measured on the pseudo-color infrared image according to a method by Simon et al. (*33*). Briefly, the infrared image of each identified particle was located with the OMNIC Picta depending on its x, y coordinates. Based on the polymer assignment, the infrared image was highlighted in the specific band region of the assigned polymer. Band regions for distinguishing polymer types were provided by Löder et al. (*34*). Then, all neighbor pixels showing the same polymer assignment were confirmed and recognized as the same particle. By observing the pseudo-color image, the

boundary of the particle, which shows significant contrast with the ambient pixels, can be clearly determined (Fig. S3). The particle dimensions were measured with the ruler tool in the OMNIC Picta software. In this study, the uncertainty of plastic size measured on infrared images lies within 5 μm when comparing to particle images obtained in the visible wavelengths. However, such an uncertainty would not cause a significant error in the particle size distribution.

The aspect ratio of the SMP, a measure of particle shape, can be estimated by calculating the ratio of the minor and major axes. To estimate the mass of the identified plastic particle, each SMP was assumed to be an ellipsoid. Based on the ellipsoid volume model (*35*), the volume of SMP was calculated using the major (a), minor (b), and intermediate (c) axes:

$$V = {\pi abc}/{6}\text{ , (1)}$$

The intermediate axis (c) of each SMP was estimated by multiplying the minor axis and the median aspect ratio (0.67 ± 0.12) of all SMP (*33*). The mass of SMP was calculated from the volume and the density (ρ, Table S5) of the assigned plastic type: $Mass_{MP} = \rho V$. (2).

Theoretical Sinking Rates of SMP. Because of their small sizes, SMP particles (n=148) in our study, which are heavier than the averaged seawater density of the top 200 m, are characterized by low Reynolds numbers. Therefore, the theoretical sinking velocities (ν) of SMP particles composed of polymers denser than the seawater was calculated using the Stokes' formula:

$$\nu = 2\left(\rho_p - \rho_f\right)gR^2/9\mu\text{ , (3)}$$

where ρ_p is the density of the particles (kg m^{-3}, Table S5). ρ_f is the mean density of the seawater of the top 200 m in our study area (1.026 kg m^{-3}). g is the gravitational field strength (m s^{-2}). R, the radius of the equivalent spherical diameter, was calculated on the basis of a best-fit ellipse used in

the formula (1). μ is the dynamic viscosity of seawater (~10^{-3} kg m^{-1} s^{-1}) taken from Ardekani and Stocker (*36*).

***LMP Data Processing*.** All identified polymer particles from the Manta net samples were weighed on an analytical balance. The averaged MP mass per piece was the total weight of plastics divided by the total number and subsequently employed to estimate the plastic mass in both Manta net and MultiNet samples. Because of the wind-induced vertical mixing, MP counts collected by Manta net may underestimate the total number of buoyant plastics in the area sampled (*37*). Thus, the integrated MP abundance/mass for the top 5 m in our study area was approximated with the equation and parameters used in literature (*38*,*39*)

***Hydrodynamic data*.** The climatology of sea surface height and geostrophic current was computed using the daily data obtained from the Copernicus Marine and Environment Monitoring Service (CMEMS, http://www.marine.copernicus.eu). It has a spatial resolution of 0.25° spanning from 1993 to 2018. The Simple Ocean Data Assimilation (SODA) reanalysis version 3.4.2 (*40*) was used for constructing the depth-dependent velocity profiles. The product is available from 1980 to 2018 with a spatial resolution of 0.5° and 50 vertical levels.

The stratification of the water column was cast by the buoyancy frequency,

$$N = \sqrt{\frac{g}{\rho_f}\frac{\partial \rho}{\partial z}} \quad , (4)$$

where g is the gravitational acceleration, $\frac{\partial \rho}{\partial z}$ is the vertical gradient of the potential density, and ρ_f is the reference density defined above.

***Contamination Prevention*.** To avoid potential contamination, we employed the following protective measures (*41*): (1) Prior to the cruise, all filters were combusted at 450 °C for >5 h to

remove organic matter; (2) Aboard ship, all sample handling was conducted in a laminar flow hood (AirClean 600 Workstation; AirClean Systems), located in a dedicated, clean room with restricted entry where only natural fiber clothing was allowed; vents in this room had AirClean pre-filters taped over them to minimize dust; (3) WTS-LV filter holders were disassembled and soaked in fresh water for 20 minutes, and then thoroughly rinsed with pressurized fresh water, and finally followed by three rinses using 0.2 μm filtered MilliQ water; (4) The clean filter holders were immediately wrapped with pre-combusted foil and stored in the laminar flow hood in the clean room; (5) The laminar flow hood was cleaned and run for at least for 15 min prior to usage and all loading and removal of filters were performed in the laminar flow hood; (6) Tweezers for handling filters were rinsed with 6 nm filtered seawater (from a tangential flow filtration unit) between processing different pore sized filters; and (7) Pre-combusted 47 mm GF/A filters were exposed in the hood during filter loading and sample processing to monitor possible MP contamination. Nitrile gloves and cotton lab coats were worn during field and laboratory work.

In the laboratory at Harbor Branch Oceanographic Institute: (1) All liquids used for sample processing and analysis (e.g., Milli-Q water, potassium hydroxide solution, ethanol) were filtered through glass-fiber filters prior to use (Whatman GF/F, 0.7 μm pore size, 47 mm diam.); (2) All glass-fiber filters and glassware (e.g., beakers, bowls, scintillation vials, Pasteur pipettes) were covered with aluminum foil, and combusted at 450 °C for >5 h; (3) Steel tweezers were washed with filtered Milli-Q water and flame combusted; (4) All sample preparation was performed in the clean laminar flow under HEPA (high-efficiency particulate air) filtration; (5) Procedural blanks in the lab (n=4) were performed by exposing GF/F filters under the laminar flow when extracting particles from QM-A filters. After the analysis of samples, these four laboratory controls together with four onboard blanks were processed employing the identical procedure as the pump samples. The resultant particles were concentrated on Anodisc filters and scanned by FTIR imaging.

***Statistical evaluation*.** Given that the datasets were not normally distributed (Kolmogorov-Smirnov test), and their variances were not homogeneous (Levene's test), the nonparametric Kruskal-Wallis statistical test was used for multiple comparisons. If the test was significant, pair-wise comparisons were performed using the nonparametric Mann-Whitney-Wilcoxon test. Values of $P < 0.05$ were considered significant. A generalized additive model (GAM) was used to estimate the relationship between the length and the aspect ratio of the identified SMP. All statistical tests and graphs were performed using R software (v.3.4.3, R Development Core Team).

Results

Contamination Controls. The analysis results of µFTIR images of procedural blanks showed no positive signals of SMP at Stations B, C and D. One polyurethane particle was confirmed at Station A. In addition, 38 polyacetal particles, determined to originate from WTS-LV pump heads, were identified on 17 out of 48 (35.4%) QM-A filters. The maximum quantity of polyacetal particles detected on a sub-filter was nine, and that was detected at 10 m depth of Station A (*SI Appendix*, Table S3). The size of polyacetal MP ranged from 25.6 to 3778.3 µm. The spectra of polyacetal particles are shown in the Fig. S4 (*SI Appendix*). In subsequent data analysis, the number of observed plastics in blanks at each station was subtracted from all datasets of pump samples corresponding to the same station.

LMP and SMP Abundance. In total, 1406 presumptive plastic particles were recovered in the Manta net samples. In a subsample of these particles (n = 457), 452 particles were confirmed as plastics and five could not be classified. The total weight of the Manta net collected particles identified as LMP (n = 452) was 0.619 g, with the averaged LMP mass per particle calculated as

0.0014 g. Wind-corrected LMP abundance in the upper 5 m of the SASG varied across the Manta net tow stations, with a range of 0.4-3.0 n m^{-3} (0.6×10^3-4.3×10^3 µg m^{-3}) and an average of 1.5 n m^{-3} (2.1×10^3 µg m^{-3}). The highest abundance was recorded at Station MT-14 (3.0 n m^{-3}; 4.3×10^3 µg m^{-3}), followed by Stations MT-16 (2.5 n m^{-3}; 3.5×10^3 µg m^{-3}), MT-18 (0.8 n m^{-3}; 1.1×10^3 µg m^{-3}), MT-22 (0.7 n m^{-3}; 0.9×10^3 µg m^{-3}), with the lowest abundance recorded at Station MT-05 (0.4 n m^{-3}; 0.6×10^3 µg m^{-3}). These findings display a general increase in the LMP abundance with proximity to the inner accumulation zone (Fig. 1).

LMP (n = 21) was found in eight out of 15 MultiNet bags at different depths (range 5-60 m, *SI Appendix*, Table S1). LMP abundances were from 0 to 1.1×10^{-2} n m^{-3} (0-15.3 µg m^{-3}) (Fig. 2 A, B, C). Disparities, spanning from 2.4 to over 5 orders of magnitude, were found in the numerical abundances of plastics when comparing SMP from WTS-LV pump to LMP from MultiNet samples in the upper 60 m. After correction of control values and subtraction of all polyacetal polymer signal from our WTS-LV pump samples, SMP particles were detected in 34 of 48 analyzed subsamples. A total of 229 particles were confirmed as plastic polymers by µFTIR imaging. The SMP abundance profiles ranged from 0-244.3 n m^{-3} and 0-20.83 µg m^{-3} (Fig. 2). No plastics were found at the depth of 3490 m at Station B. SMP abundances were highly variable in our four vertical profiles (Kruskal-Wallis test, $P < 0.05$, *SI Appendix*, Table S4), with the highest mean abundance detected at 10 m at Station A (218.3 ± 45.1 n m^{-3}), followed by 60 m at Station D (85.4 ± 9.5 n m^{-3}), and 4835 m at Station C (71.1 ± 21.5 n m^{-3}) (Fig. 2 A, C, D). Generally, SMP abundances in the vertical profiles decreased with depth, except at Station C (Fig. 2C). In the upper 60 m, the mean abundance of SMP in the outer accumulation zone (Stations A and D, mean: 105.3 ± 93.9 n m^{-3}, median: 85.4 n m^{-3}) was significantly higher than samples taken from the inner accumulation zone (Stations B and C, mean: 24.4 ± 24.8 n m^{-3}, median: 17.1 n m^{-3} (Mann-Whitney-Wilcoxon test, W = 85, $P = 0.026$, *SI Appendix*, Fig. S5).

Polymer Composition. A total of 12 polymer types, including theoretically buoyant polymers, were identified in the SMP samples (*SI Appendix*, Fig. S6). Five polymer types accounted for more than 80% of the particle count, including polyamide 6/6.6 (PA 6/6.6, 29.3%, n=67), alkyd resin (16.2%, n=37), PP (15.3%, n=35), PE (11.0%, n=25) and polyethylene/polypropylene copolymer (PE/PP, 8.7%, n=20). The polymer species of each pump sample differed, ranging from 0 to 10 polymer types. PE, PP, PE/PP and Ethylene-ethyl acrylate copolymer (EEA) particles that are lighter than the *in-situ* seawater (~1.025 g cm^{-3}) were also detected in the ocean's interior (Fig. 3 and *SI Appendix*, Table S5). In the Manta net LMP subsamples, PE was the dominant polymer, corresponding to 79.2% (n = 358) of the particles, followed by PP (12.2%, n = 55) and PE/PP copolymer (7.3%, n = 33). The 1.3% remaining particles (n = 6) were identified as PA 6/6.6 (n = 3), polyester (n = 2) and polystyrene (PS, n = 1).

Size and Theoretical Sinking Rates of SMP. The length of SMP particles ranged from 20.1 to 321.2 μm (mean = 58.6 ± 32.4 μm, median = 49.6 μm), while the width spanned from 15.9 to 126.3 μm (mean = 35.3 ± 11.6 μm, median = 35.5 μm, Fig. S7). A total of 25% (n = 57) in the length and 88% (n = 202) in the width of all identified plastic particles were less than 40 μm long (SS mesh pore size), while 62% (length) and 97% (width) of particles were <56.6 μm (the theoretical diagonal of square SS mesh sieve aperture). The aspect ratio of particles steadily increased with decreases in length (GAM, $R^2 = 0.63$, $P << 0.01$, *SI Appendix*, Fig. S8) indicating smaller particles became spherical. The theoretical sinking velocity of SMP particles (n = 148) with densities higher than seawater ranged from 2.4×10^{-9} to 1.0×10^{-6} m s^{-1}(Table S6).

Oxidation Degree. In the Manta net samples, PE-LMP from the outer accumulation zone (n = 99) of the SASG exhibited modestly higher carbonyl indices in contrast to PE-LMP (n = 259)

from the inner accumulation zone (Mann-Whitney-Wilcoxon test, W = 8738, $P = 1.6 \times 10^{-6}$, Fig. 4A). Overall, PE-SMP from WTS-LV pump samples presented significantly higher carbonyl indices than those captured in Manta nets from the identical sampling region within the SASG (Mann-Whitney-Wilcoxon test, the outer accumulation zone, W = 479, $P = 9.3 \times 10^{-4}$; the inner accumulation zone, W = 27, $P = 1.4 \times 10^{-6}$, Fig. 4A).

Discussion

This study provides the first dataset on the distribution of MP throughout the water column beneath an offshore plastic accumulation zone. Although the dataset is modest and comes from a single expedition, the abundance and composition of MP at different depths from our study provide unique insight into how MP are distributed from the epi- to the abyssopelagic layer within the SASG. Overall, we observed that LMP abundances in net samples (Manta net and MultiNet) were at least two orders of magnitude lower than the SMP abundances concurrently sampled with *in-situ* pumps (Fig. 2, refer to Table S1 for the exact abundance values). These disparities between abundances in the pump and net samples confirm that smaller-sized MP has been largely undercounted and is an important contributor to plastic mass balance in the SASG. Our surface SMP abundances are comparable to existing data (13-501 n m^{-3}) from surface waters of the North Atlantic Ocean by Enders et al. (*16*), who used Raman spectroscopy to identify MP down to 10 µm and found over 64% of particles were less than 40 µm. In comparison to a recent study that employed similar large-volume sampling and automated interpretation µFTIR imaging methods to study the plastic pollution in the deep-water column, SMP abundance (0-244.3 n m^{-3}, median: 25.6 n m^{-3}) in our study was higher than reported for the Arctic Ocean (size fraction: 25-50 µm, abundance: 0-96 n m^{-3}, median: 13.0 n m^{-3}) (*18*). It has been shown that smaller-sized MP (typically <150 µm) can translocate into the tissues and organs of organisms upon ingestion, exerting potential negative impacts on marine organisms (*19*). Investigation of smaller-sized

plastics, largely missed in net-based and visual detection-based collections, is pivotal to understanding the ecological impacts of plastic debris as a whole in the ocean ecosystem.

Horizontal Distribution. Floating plastic debris is generally understood to increase in abundance towards the center of oceanic gyres (*3-5*). In the SASG, Cózar et al. (*4*) reported differences of a hundred-fold in plastic concentration (>200 μm) between debris within inner and outer accumulation zones, which agree with our Manta net data (Fig. 1). Our observations of lower SMP abundances at water depths <60 m in the inner SASG accumulation zone (Stations B and C) was observed, compared to those in the outer accumulation zone (Stations A and D) (Mann-Whitney-Wilcoxon test, $P < 0.05$, Fig. 2, *SI Appendix*, Fig. S2) are seemingly conflicting with these previous observations. In particular, Station A has the highest abundance of SMP, followed by Stations D, B and C. At present, we are not able to interpret this mismatch with certainty. However, known processes provide a possible explanation for this anomaly. A previous modelling study predicted that 60%-80% of floating debris in the South Atlantic accumulation zone was from South America (*42*). As the basin-scale circulation largely flows along the isolines of sea surface height, this floating debris from the western border of the South Atlantic would likely arrive first at Station B, followed by Stations A, D and finally Station C (Fig. 5). The floating plastics probably disperses along the proposed route, which may partially contribute to the lower SMP numbers in the near-surface layer of Station C. Additionally, the velocity fields and sea level anomalies on the sampling day of each station (*SI Appendix*, Fig. S9) showed that Stations A and D were closer to the core of the anticyclonic eddies than Stations B and C. Previous model results documented that particles were prone to aggregate at the edges of the anticyclonic eddies (*43*). Based on a MP field survey in the North Atlantic Gyre, data from satellite observations and models, Brach et al. (*44*) provided evidence that the anticyclonic eddies could retain, concentrate, and transport MP. High accumulations of near-surface SMP at Stations

A and D might also be closely related to these meso- and submesoscale features (Fig. S9). More extensive *in-situ* observations of plastics in the water column will be necessary to resolve the temporal-spatial patterns of water-column MP and verify the possible mechanisms at play.

Vertical profiles. Contrasting profile distribution patterns of MP were observed in the Arctic Ocean among four stations by Tekman et al. (18), who regarded the inconsistent vertical distributions among stations as indications for different mechanisms in the MP flux, highlighting the role of local ocean circulation in the distribution of MP. Similar vertical differences were also observed in our study. SMP abundances at Stations (A, B, D) generally decreased with depth, but contrary to this trend, Station C showed a striking increase of over 20-fold (Fig. 2) at depth. To compare this with the current velocity structure at each station, we computed the climatological depth-dependent velocity profile at the closest grid point of the Simple Ocean Data Assimilation database in 1993-2018 (Fig. 4B). It clearly indicates that the near bottom velocity of bottom currents at Station C was 2-4 times weaker than the other three Stations A, B, and D. We hypothesize that the slower bottom current velocity at Station C was less dilutive and appears to be entraining SMP particles transported to this depth. Although the concurrent presence of both high-abundance SMP and slow currents was only observed at one station, it agrees well with Kane et al. (*45*) who reported that low intensity currents may accumulate plastic debris in the Tyrrhenian Sea based on a combination of *in-situ* MP measurements and numerical modelling. The accumulation of SMP at depth may also be attributed to the interactions with biological processes (e.g., biofouling, marine aggregate formation and incorporation into fecal pellets), which have been shown to accelerate the downward transport of plastics (*46*, *47*). But the knowledge of water-column MP interactions with biological processes is limited and warrants further research. Additionally, the three-dimensional transportation of plastic particles might contribute to the observed distribution patterns of SMP along the depth continuum (*6*). Non-

metric multidimensional scaling ordination analysis of the polymer composition at each depth supports the clustering of samples into three distinct groups (Fig. 4C, analysis of similarities R=0.32, p=0.005). In general, high similarity of polymer types between the deep samples and surface samples at different stations (Fig. 4C) was observed, which suggests oceanic SMP particles are dispersed in lateral advection, vertical convection, or a combination of these movements. Further studies of vertical measurements will aid in the understanding of MP transport pathways in the water column.

Steep density gradients, termed pycnoclines, are known to considerably decelerate settling rates of particles (such as suspended solids, algae or detritus, marine snow, etc.) and prolong their residence times above or within the pycnocline, resulting in a preferential accumulation (*48, 49*). Recently, several studies have reported higher abundances of MP particles in the pycnocline layers (*14, 50, 51*). In this study, we deliberately placed high volume pumps within the pycnocline at each station to investigate this phenomenon. At our sampling stations, the maximum buoyancy frequency values (0.021-0.025 s^{-1}, Fig. S10) were larger than 0.016 s^{-1}, indicating that the local stratified layers were well-defined (*32*). Stratified conditions such as these have been observed to entrap marine snow (≥200 μm) particles (*48*), yet we only saw a modest peak in pycnocline SMP numbers at one (Station B) of the four sampling stations. It should be noted that Station B displayed the most intense pycnocline conditions from our sample set. However, LMP abundances were observed to increase within pycnocline proximity in the MultiNet samples, particularly MN-01 and -02 (Fig. 2). This difference may reside in the smaller particle size of SMP investigated in this study compared to previous studies (*14, 50, 51*), whose detectable sizes were limited to MP larger than 100 μm. The retention time of particles at ocean pycnoclines, increases quadratically with particle size (*52*), with stratification effects being assessed by comparing the size of settling objects with the fundamental length scale O (100 μm to 1 mm).

Thus, objects smaller than 100 μm are much less influenced by water stratification (*36, 53*). Moreover, the theoretically predicted sinking velocities (2.4×10^{-9} to 1.0×10^{-6} m s^{-1}) of SMP particles in our study were at least three orders of magnitude smaller than previously measured settling speeds (1.0×10^{-3} to 250×10^{-3} m s^{-1}) of large MPs (>300 μm) and fecal pellets (*SI Appendix*, Table S6). Notably, SMP size are much smaller than microplastics and fecal pellets of which the settling speeds were previously measured. These extremely low settling velocities of SMP imply higher dispersion, even distribution, and longer lifetime in the water column. Altogether, these factors could explain the lack of retention of SMP particles at isopycnal interfaces. However, the sinking behaviors of SMP may be altered by microbial colonization or incorporation into marine snow and fecal pellets of zooplankton (*46, 47*). Incorporation of SMP into egested organic materials and marine aggregates, could significantly increase the settling velocity of plastic particles and thus enhance their export from oceanic surface layers and sinking to the seafloor (*46*), which could result in the reduction of plastic abundances in the upper water column. This undercounting seems especially true with respect to plastics that are denser than the ambient seawater. In contrast, buoyant plastics may be less influenced because these particles can resurface upon aggregate disintegration (*54*).

Chemical Characteristics of Polymer Particles. The polymer compositions of plastics in WTS-LV pump samples and Manta net samples varied significantly. Overall, PE and PP (91.4%) dominated in the trawl samples, in agreement with findings extensively documented in the literature (*4, 5, 7*). In contrast, the polymers in the WTS-LV pump samples included PA 6/6.6 (29.1%), alkyd resin (16.1%) and polyolefins (PP: 15.2% and PE:10.9%, PE/PP: 8.7%). This incongruity between polymer types collected from pump and Manta net samples verify plastic compositional changes with sampling depth due to size variation, buoyancies and chemical properties of specific polymers. The prevalence of PA in the pelagic water column has also been

548 reported in the Arctic and Pacific Oceans (*14*, *18*). PA is a typical polymer used for fishing nets
549 and ropes. The high number of PA particles indicates that active fisheries in the South Atlantic
550 Ocean (*55*), may be a sea-based source of PA plastics. Plastic debris sourced from the fishing and
551 other marine activities accounted for over 70% of marine plastic litter by mass on a remote island
552 in the central South Atlantic Ocean (*56*). Furthermore, polymers with functional groups, like the
553 amide bonds in PA, are susceptible to degradation such as biotransformation and disintegration,
554 relative to more recalcitrant polymers such as PE (*57*, *58*). Enhanced susceptibility to general
555 degradation would accelerate generation of SMP from larger pieces, which could contribute to the
556 higher abundance of smaller PA in the marine environment. The second most abundant polymer
557 type found in our study was alkyd resin. The dominant alkyd resin in marine environments is
558 likely linked to the degradation of the painted surfaces of metal ships (*23*, *59*). As an increasingly
559 busy shipping route from South America to Asia, and a fishing hotspot (*55*, *60*), the South
560 Atlantic Ocean is reasonably susceptible to these paints shedding from commercial and fishery
561 vessels. Ship paints have been shown to disintegrate more rapidly when compared with other
562 plastic polymers and this observation could explain their smaller size distribution in our samples
563 (*23*, *59*).
564
565 The overall inventory from our WTS-LV pumps shows abundant plastic particles smaller than
566 100 μm below the surface of the South Atlantic (*SI Appendix*, Fig. S4). Our pump sampling
567 method was selective for particles that passed through the 40 μm mesh and the size distribution of
568 SMP shows a peak in abundance of fragments around 40 μm (Fig. S4), suggesting the meshes
569 were efficiently selecting for SMP. Meanwhile, SMP abundance peaking around 40 μm also
570 implied that SMP size was not apparently altered by our sample processing steps such as frozen
571 storage at -80°C, water bath sonication treatments and centrifugations. However, several large
572 plastics (>100 μm) were observed in the 2-40 μm size fraction. A similar phenomenon was

reported in a previous study where a 333 μm neuston net sampling yielded over 60% of non-string-like MP (0.4-1.0 mm) was able to pass through the mesh (*61*). A possible explanation for the observed size anomaly is the pre-combusted stainless-steel mesh (40 μm) may be deformed under increasing pressure during sampling, allowing larger particles through the mesh. Larger and softer plastic particles could also have worked their way through the 56.6 μm minimal theoretical diagonal of the square SS mesh sieve aperture. Finally, but less likely, the presence of larger plastic particles may also be the result of the overlay or aggregation of small particles during the processing of the samples. For instance, samples were concentrated on the 25 mm Anodisc membrane which was assembled in an open-face 13 mm filter holder, and finally generated an effective filtration area of 133 mm^2 (~13 mm in diameter) for μFTIR imaging, which may lead to particles overlaying. It should be mentioned that the boundary geometry of SMP particles measured by this approach suffers from uncertainties, to some extent. The uncertainty in the SMP dimension measurement can be attributed to the low peak-signal-to-noise ratios, which are caused by the irregularities of particle morphology (*34*), inhomogeneity in chemical composition of plastic materials, or insufficiently removed biofilm (*62*).

Manta net collected PE-LMP from the outer accumulation zone had higher carbonyl indices than from the inner accumulation zone (Fig. 4A) suggesting a longer residence time for these LMP. However, this finding is in disagreement with previous research (*63*, *64*), that reported plastic particles displaying a higher degree of oxidation offshore along a transect. A possible explanation for this discrepancy is that the literature datasets were from the inshore to offshore samples, in contrast to all samples from the SASG in our study, where plastic particles with different oxidative history were entrapped and move with the flow in the gyre. Therefore, it is plausible that PE-LMP retained in the gyre for a longer time was coincidentally captured in the outer accumulation zone. Higher carbonyl indices were observed for SMP collected by WTS-LV

598 pumps compared to LMP collected with Manta nets, suggesting SMP were potentially more
599 degraded than LMP. A similar result was obtained by Ter Halle et al. (65), who found a
600 significant decrease in the molar mass from mesoplastic to MP sampled from the North Atlantic
601 Gyre, which suggests that small plastics are more oxidized than larger ones. These data also agree
602 with previous findings for the model of plastic degradation, which denotes that plastic degrades
603 into smaller fragments and these daughter fragments are likely to be more oxidized than parent
604 fragments due to their different chemical and physical properties (*2*). It should be noted that
605 specific polymer types exhibit variation in carbonyl indices, which underlines the need for a
606 larger database and development of other reliable methods to evaluate the weathering degree of
607 plastics in the environment.
608
609 The appreciable amounts of SMP in the ocean's interior unveiled here suggest a potential
610 ecosystem-wide impact. Compared to LMP, SMP are more readily ingested by marine particle
611 feeders because of their small size and the smaller-sized plastic has the ability to translocate to
612 internal tissues in organisms (*66*), resulting in bioaccumulation of MP and its associated
613 chemicals at multiple trophic levels (*67*). Methods for the quantification of water-column SMP in
614 the open ocean is new and results are therefore relatively uncommon, however, the current study
615 together with two previous studies all revealed unexpectedly high numbers of SMP in the ocean's
616 interior and varied with depth (*18, 22*). Previous reports have estimated mean MP abundances in
617 the upper 200 m of an Atlantic North-South transect as high as 2272 n m^{-3} (*22*). Based on all these
618 depth-resolved observations, it is reasonable to consider the following scenario: large amounts of
619 SMP accumulate at certain depths, forming a high plastic-to-marine biota ratio, thus increasing
620 the probability of encountering and ingesting plastic particles by marine organisms (*14, 68*). For
621 instance, comparing our measured SMP abundances (0-244.3 n m^{-3}) to previously measured total
622 copepod abundance (0-12 n m^{-3}) at depth of 0-3000 m (*69*) in the South Atlantic, it is plausible

623 that copepods would encounter these abundant plastics at certain depths. Furthermore, the impacts
624 of SMP on marine fauna could be exacerbated by the combination of more aged surface
625 properties and large-aspect ratios (*SI Appendix*, Fig. S5), both of which have been experimentally
626 documented to enhance MP ingestion (*47, 70*). Filed evidence showed that MP (40-200 μm)
627 constituted roughly 26% of all plastic particles ingested by mesopelagic fishes in the northwest
628 Atlantic Ocean (*71*), and 45% of deep-sea benthic amphipods in the North East Atlantic contained
629 translocated MP in soft tissues, of which PA was the dominant polymer type consistently found
630 (*72*). As commercial fishing efforts scale up to harvest marine species for human consumption,
631 studies focusing on smaller MP ingestion are urgently needed to assess the extent of plastic
632 contamination in biomass, which may represent a large fraction of the 'missing' plastics (*73*).
633 Marine organisms grazing on MP also have potential impacts on global biogeochemical cycling.
634 Employing an Earth system model, Kvale et al (*74*) predicted that zooplankton ingesting
635 microplastics could accelerate global deoxygenation by an extra 0.2-0.5% relative to 1960 values
636 by the year 2020 and reduce the oxygen inventory in the North Pacific by up to 10%.
637
638 Our results show that highly abundant SMP dominate surface to near-seafloor waters in the
639 plastic accumulation zone of the South Atlantic and form microplastic hotspots at certain depths,
640 implicating the ocean interior as a crucial pool of 'missing' plastics, particularly in low-flow
641 regimes. The abundances and distributions patterns of SMP varied geographically and vertically
642 due to the diverse and complex redistribution processes interacting with different plastic particles.
643 Compared with net-collected LMP, SMP particles are more highly oxidized and appear to have a
644 longer lifetime in the water column, suggesting increased marine ecosystem health risks through
645 possible bio-uptake of plastic particles and associated chemicals (*75*) and potential impacts to
646 global biogeochemical cycles (*74*). SMP are distinguished from LMP with respect to their high
647 abundance, chemical nature, transport behavior, weathering stages, interactions with ambient

environments, bioavailability and the release efficiency of plastic additives (*57*). These distinct characteristics impact their environmental fate and potential impacts on marine ecosystems. Given the fundamental elements of our findings, this study of the SASG strongly suggests that SMP, largely unaccounted for in previous studies, is a critical and unique component in ocean plastic inventories. Additionally, our study provides a stimulus for additional work to interpret and understand the fate and potential impacts of microplastics in aquatic systems in general.

References

1. S. B. Borrelle *et al.*, Predicted growth in plastic waste exceeds efforts to mitigate plastic pollution. *Science* **369**, 1515-1518 (2020).
2. A. L. Andrady, The plastic in microplastics: A review. *Marine pollution bulletin* **119**, 12-22 (2017).
3. E. Van Sebille *et al.*, A global inventory of small floating plastic debris. *Environmental Research Letters* **10**, 124006 (2015).
4. A. Cózar *et al.*, Plastic debris in the open ocean. *Proceedings of the National Academy of Sciences* **111**, 10239-10244 (2014).
5. M. Eriksen *et al.*, Plastic pollution in the world's oceans: more than 5 trillion plastic pieces weighing over 250,000 tons afloat at sea. *PloS One* **9**, e111913 (2014).
6. E. Van Sebille *et al.*, The physical oceanography of the transport of floating marine debris. *Environmental Research Letters* **15**, 023003 (2020).
7. K. L. Law *et al.*, Plastic accumulation in the North Atlantic subtropical gyre. *Science* **329**, 1185-1188 (2010).
8. M. Bergmann, M. B. Tekman, L. Gutow, Marine litter: Sea change for plastic pollution. *Nature* **544**, 297 (2017).

9. L. C. Woodall *et al.*, The deep sea is a major sink for microplastic debris. *Royal Society Open Science* **1**, 140317 (2014).
10. F. Pohl, J. T. Eggenhuisen, I. A. Kane, M. A. Clare, Transport and burial of microplastics in deep-marine sediments by turbidity currents. *Environmental Science & Technology* **54**, 4180-4189 (2020).
11. B. H. Robison, Conservation of deep pelagic biodiversity. *Conservation Biology* **23**, 847-858 (2009).
12. L. A. Levin *et al.*, Global observing needs in the deep ocean. *Frontiers in Marine Science* **6**, 241 (2019).
13. K. K. La Daana *et al.*, Microplastics in sub-surface waters of the Arctic Central Basin. *Marine Pollution Bulletin* **130**, 8-18 (2018).
14. C. A. Choy *et al.*, The vertical distribution and biological transport of marine microplastics across the epipelagic and mesopelagic water column. *Scientific Reports* **9**, 7843 (2019).
15. P. S. Ross *et al.*, Pervasive distribution of polyester fibres in the Arctic Ocean is driven by Atlantic inputs. *Nature Communications* **12**, 106 (2021).
16. K. Enders, R. Lenz, C. A. Stedmon, T. G. Nielsen, Abundance, size and polymer composition of marine microplastics≥ 10 μm in the Atlantic Ocean and their modelled vertical distribution. *Marine Pollution Bulletin* **100**, 70-81 (2015).
17. C. Lorenz *et al.*, Spatial distribution of microplastics in sediments and surface waters of the southern North Sea. *Environmental Pollution* **252**, 1719-1729 (2019).
18. M. B. Tekman *et al.*, Tying up loose ends of microplastic pollution in the Arctic: Distribution from the sea surface, through the water column to deep-sea sediments at the HAUSGARTEN observatory. *Environmental Science & Technology*, **54**, 4079-4090 (2020).

19. A. Lusher, P. Hollman, J. Mendoza-Hill, “Microplastics in fisheries and aquaculture: status of knowledge on their occurrence and implications for aquatic organisms and food safety” (FAO Fisheries and Aquaculture Technical Paper No. 615. Rome, Italy, 2017).
20. GESAMP, “Sources, fate and effects of microplastics in the marine environment: part two of a global assessment” (GESAMP No. 93, International Maritime Organization, London, 2016).
21. A. Ter Halle *et al.*, Nanoplastic in the North Atlantic subtropical gyre. *Environmental Science & Technology* **51**, 13689-13697 (2017).
22. K. Pabortsava, R. S. Lampitt, High concentrations of plastic hidden beneath the surface of the Atlantic Ocean. *Nature Communications* **11**, 4073 (2020).
23. A. L. d. F. Lacerda *et al.*, Plastics in sea surface waters around the Antarctic Peninsula. *Scientific Reports* **9**, 1-12 (2019).
24. J. K. Bishop, P. J. Lam, T. J. Wood, Getting good particles: Accurate sampling of particles by large volume in-situ filtration. *Limnology and Oceanography: Methods* **10**, 681-710 (2012).
25. S. Primpke, M. Wirth, C. Lorenz, G. Gerdts, Reference database design for the automated analysis of microplastic samples based on Fourier transform infrared (FTIR) spectroscopy. *Analytical and Bioanalytical Chemistry* **410**, 5131-5141 (2018).
26. J. A. Brandon, A. Freibott, L. M. Sala, Patterns of suspended and salp-ingested microplastic debris in the North Pacific investigated with epifluorescence microscopy. *Limnology and Oceanography Letters* **5**, 46-53 (2020).
27. J. A. Brandon, M. Goldstein, M. D. Ohman, Long-term aging and degradation of microplastic particles: Comparing in situ oceanic and experimental weathering patterns. *Marine Pollution Bulletin* **110**, 299-308 (2016).

28. L. Canopoli, F. Coulon, S. T. Wagland, Degradation of excavated polyethylene and polypropylene waste from landfill. *Science of the Total Environment* **698**, 134125 (2020).

29. A. Moldovan, R. Buican, S. Patachia, M. Tierean, Characterization of polyolefins wastes by FTIR spectroscopy. *Bulletin of the Transilvania University of Brasov. Engineering Sciences. Series I* **5**, 65 (2012).

30. A. Mendoza, G. Kortaberria, F. F. Marzo, U. Mayor, O. C. Basurko, C. Peña-Rodriguez, Solvent-Based Elimination of Organic Matter from Marine-Collected Plastics, *Environments* **8**, 68 (2021).

31. A. I.Catarino, V. Macchia, W. G. Sanderson, R. C.Thompson, T. B. Henrya, Low levels of microplastics (MP) in wild mussels indicate that MP ingestion by humans is minimal compared to exposure via household fibres fallout during a meal, *Environmental Pollution* **237**, 675-684 (2018).

32. J. C. Prata *et al*., Preparation of biological samples for microplastic identification by Nile Red. *Science of The Total Environment* **783**, 147065 (2021).

33. M. Simon, N. van Alst, J. Vollertsen, Quantification of microplastic mass and removal rates at wastewater treatment plants applying Focal Plane Array (FPA)-based Fourier Transform Infrared (FT-IR) imaging. *Water Research* **142**, 1-9 (2018).

34. M. G. J. Löder, M. Kuczera, S. Mintenig, C. Lorenz, G. Gerdts, Focal plane array detector-based micro-Fourier-transform infrared imaging for the analysis of microplastics in environmental samples. *Environmental Chemistry* **12**, 563-581 (2015).

35. R. G. Kumar, K. B. Strom, A. Keyvani, Floc properties and settling velocity of San Jacinto estuary mud under variable shear and salinity conditions. *Continental Shelf Research* **30**, 2067-2081 (2010).

36. A. Ardekani, R. Stocker, Stratlets: low Reynolds number point-force solutions in a stratified fluid. *Physical Review Letters* **105**, 084502 (2010).

37. T. Kukulka, G. Proskurowski, S. Morét-Ferguson, D. Meyer, K. Law, The effect of wind mixing on the vertical distribution of buoyant plastic debris. *Geophysical Research Letters* **39**, (2012).

38. M. Egger, F. Sulu-Gambari, L. Lebreton, First evidence of plastic fallout from the North Pacific Garbage Patch. *Scientific Reports* **10**, 7495 (2020).

39. J. Reisser *et al.*, The vertical distribution of buoyant plastics at sea: an observational study in the North Atlantic Gyre. *Biogeosciences* **12**, 1249-1256 (2015).

40. J. A. Carton, G. A. Chepurin, L. Chen, SODA3: A new ocean climate reanalysis. *Journal of Climate* **31**, 6967-6983 (2018).

41. S. Zhao, M. Danley, J. E. Ward, D. Li, T. J. Mincer, An approach for extraction, characterization and quantitation of microplastic in natural marine snow using Raman microscopy. *Analytical Methods* **9**, 1470-1478 (2017).

42. L.-M. Lebreton, S. Greer, J. C. Borrero, Numerical modelling of floating debris in the world's oceans. *Marine Pollution Bulletin* **64**, 653-661 (2012).

43. A. Samuelsen, S. S. Hjøllo, J. A. Johannessen, R. Patel, Particle aggregation at the edges of anticyclonic eddies and implications for distribution of biomass. *Ocean Science* **8**, 389-400 (2012).

44. L. Brach *et al.*, Anticyclonic eddies increase accumulation of microplastic in the North Atlantic subtropical gyre. *Marine Pollution Bulletin* **126**, 191-196 (2018).

45. I. A. Kane *et al.*, Seafloor microplastic hotspots controlled by deep-sea circulation. *Science* **368**, 1140-1145 (2020).

46. L. A. Amaral-Zettler, E. R. Zettler, T. J. Mincer, M. A. Klaassen, S. M. Gallager, Biofouling impacts on polyethylene density and sinking in coastal waters: A macro/micro tipping point? *Water Research*, 117289 (2021).

47. S. Zhao, J. E. Ward, M. Danley, T. J. Mincer, Field-based evidence for microplastic in marine aggregates and mussels: implications for trophic transfer. *Environmental Science & Technology* **52**, 11038-11048 (2018).
48. S. MacIntyre, A. L. Alldredge, C. C. Gotschalk, Accumulation of marines now at density discontinuities in the water column. *Limnology and Oceanography* **40**, 449-468 (1995).
49. M. M. Mrokowska, Influence of pycnocline on settling behaviour of non-spherical particle and wake evolution. *Scientific Reports* **10**, 20595 (2020).
50. M. Zobkov, E. Esiukova, A. Zyubin, I. Samusev, Microplastic content variation in water column: The observations employing a novel sampling tool in stratified Baltic Sea. *Marine Pollution Bulletin* **138**, 193-205 (2019).
51. E. Uurasjärvi, M. Pääkkönen, O. Setälä, A. Koistinen, M. Lehtiniemi, Microplastics accumulate to thin layers in the stratified Baltic Sea. *Environmental Pollution* **268**, 115700 (2021).
52. K. Kindler, A. Khalili, R. Stocker, Diffusion-limited retention of porous particles at density interfaces. *Proceedings of the National Academy of Sciences* **107**, 22163-22168 (2010).
53. A. Doostmohammadi, R. Stocker, A. M. Ardekani, Low-Reynolds-number swimming at pycnoclines. *Proceedings of the National Academy of Sciences* **109**, 3856-3861 (2012).
54. M. Kooi, E. H. van Nets, M. Scheffer, A. A. Koelmans, Ups and downs in the ocean: Effects of biofouling on vertical transport of microplastics. *Environmental Science & Technology* **51**, 7963-7971 (2017).
55. T. A. Clay *et al.*, A comprehensive large-scale assessment of fisheries bycatch risk to threatened seabird populations. *Journal of Applied Ecology* **56**, 1882-1893 (2019).
56. P. G. Ryan, The transport and fate of marine plastics in South Africa and adjacent oceans. *South African Journal of Science* **116**, 1-9 (2020).

57. B. Gewert, M. M. Plassmann, M. MacLeod, Pathways for degradation of plastic polymers floating in the marine environment. *Environmental Science: Processes & Impacts* **17**, 1513-1521 (2015).
58. K. Min, J. D. Cuiffi, R. T. Mathers, Ranking environmental degradation trends of plastic marine debris based on physical properties and molecular structure. *Nature Communications* **11**, 727 (2020).
59. Y. K. Song, S. H. Hong, M. Jang, G. M. Han, W. J. Shim, Occurrence and distribution of microplastics in the sea surface microlayer in Jinhae Bay, South Korea. *Archives of Environmental Contamination and Toxicology* **69**, 279-287 (2015).
60. P. G. Ryan, B. J. Dilley, R. A. Ronconi, M. Connan, Rapid increase in Asian bottles in the South Atlantic Ocean indicates major debris inputs from ships. *Proceedings of the National Academy of Sciences* **116**, 20892-20897 (2019).
61. T. Tokai, K. Uchida, M. Kuroda, A. Isobe, Mesh selectivity of neuston nets for microplastics. *Marine Pollution Bulletin* **165**, 112111 (2021).
62. J. P. Harrison, M. Schratzberger, M. Sapp, A. M. Osborn, Rapid bacterial colonization of low-density polyethylene microplastics in coastal sediment microcosms. *BMC Microbiology* **14**, 232 (2014).
63. E. Martí *et al.*, The Colors of the Ocean Plastics. *Environmental Science & Technology* **54**, 6594-6601 (2020).
64. J. Brandon, M. Goldstein, M. D. Ohman, Long-term aging and degradation of microplastic particles: comparing in situ oceanic and experimental weathering patterns. *Marine Pollution Bulletin* **110**, 299-308 (2016).
65. A. Ter Halle *et al.*, To what extent are microplastics from the open ocean weathered? *Environmental Pollution* **227**, 167-174 (2017).

66. H. K. Mcllwraith, J. Kim, P. Helm, S. P. Bhavsar, J. S. Metzger, and C. M. Rochman, Evidence of Microplastic Translocation in Wild-Caught Fish and Implications for Microplastic Accumulation Dynamics in Food Webs. *Environmental Science & Technology* **55**, 12372-12382 (2021).

67. M. E. Miller, M. Hamann, F. J. Kroon, Bioaccumulation and biomagnification of microplastics in marine organisms: A review and meta-analysis of current data. *Plos One* **15**, eo240792 (2020).

68. J. M. Gove *et al.*, Prey-size plastics are invading larval fish nurseries. *Proceedings of the National Academy of Sciences* **116**, 24143-24149 (2019).

69. A. Vereshchaka, G. Abyzova, A. Lunina, E. Musaeva, The deep-sea zooplankton of the North, Central, and South Atlantic: biomass, abundance, diversity. *Deep Sea Research Part II: Topical Studies in Oceanography* **137**, 89-101 (2017).

70. R. J. Vroom, A. A. Koelmans, E. Besseling, C. Halsband, Aging of microplastics promotes their ingestion by marine zooplankton. *Environmental Pollution* **231**, 987-996 (2017).

71. A. M. Wieczorek *et al.*, Frequency of microplastics in mesopelagic fishes from the Northwest Atlantic. *Frontiers in Marine Science* **5**, 39 (2018).

72. W. Courtene-Jones, B. Quinn, C. Ewins, S. F. Gary, B. E. Narayanaswamy, Consistent microplastic ingestion by deep-sea invertebrates over the last four decades (1976–2015), a study from the North East Atlantic. *Environmental Pollution* **244**, 503-512 (2019).

73. K. Kvale, A. Prowe, C.-T. Chien, A. Landolfi, A. Oschlies, The global biological microplastic particle sink. *Scientific Reports* **10**, 16670 (2020).

74. K. Kvale, A. Prowe, C.-T. Chien, A. Landolfi, A. Oschlies, Zooplankton grazing of microplastic can accelaerate global loss of ocean oxygen. *Nature Communications* **12**, 2358 (2021).

75. M. MacLeod, H. P. H. Arp, M. B. Tekman, A. Jahnke, The global threat from plastic pollution. *Science* **373**, 61-65 (2021).

Acknowledgments: The authors thank the crew and scientists aboard the NIOZ RV *Pelagia* cruise 64PE448.

Funding: This work was supported by start-up funds from NIOZ to L.A. A.-Z. to help fund the expedition. Funds for this study came from: FAU World Class Faculty and Scholar Program to TJM; a NOAA marine debris grant NA17NOS9990024 awarded to L.A.A.-Z. and T.J.M., and the American Chemistry Council awarded to L.A.A.-Z., E.Z, and T.J.M.

Author Contributions: S.Z., E.R.Z, L.A.A-Z., and T.J.M. designed research; S.Z., E.R.Z., R.P.B., and L.A.A.-Z performed research; S.Z., E.R.Z., R.P.B., P.L., and T.J.M. analyzed data; S.Z. wrote the first draft of the paper, all coauthors were involved in editing subsequent versions.

Competing Interest Statement: The authors declare no competing interest.

Data and materials availability: All data needed to evaluate the conclusions in the paper are present in the paper and/or the Supplementary Materials. Additional data related to this paper may be requested from the authors.

Figures and Tables

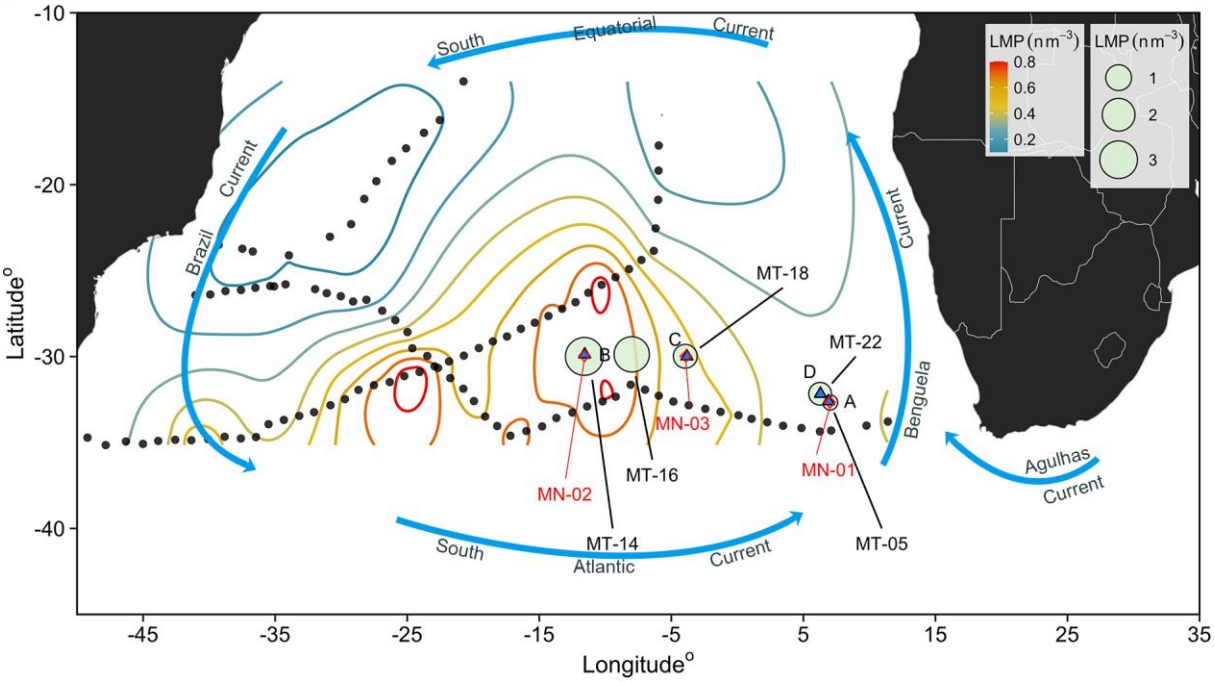

869

870 **Fig. 1. Map of the Manta net, MultiNet, and WTS-LV pumps sampling locations.** Blue
871 triangles represent four WTS-LV pump sampling stations (A, B, C, D). Green shaded bubbles
872 indicate the five Manta net tow stations (MT-05, -14, -16, -18, -22) and size of circles reflects the
873 wind-corrected LMP (0.3-5.0 mm) abundances. Red diamonds represent the three Multinet
874 sampling stations (MN-01, -02, and 03). Surface LMP abundances (n m^{-3}) in the South Atlantic
875 Ocean by Eriksen et al. (5) are contoured using the Kriging interpolation method based on the
876 surface-trawl datasets (gray dots). The blue arrows represent the schematic circulation in the
877 South Atlantic.

878

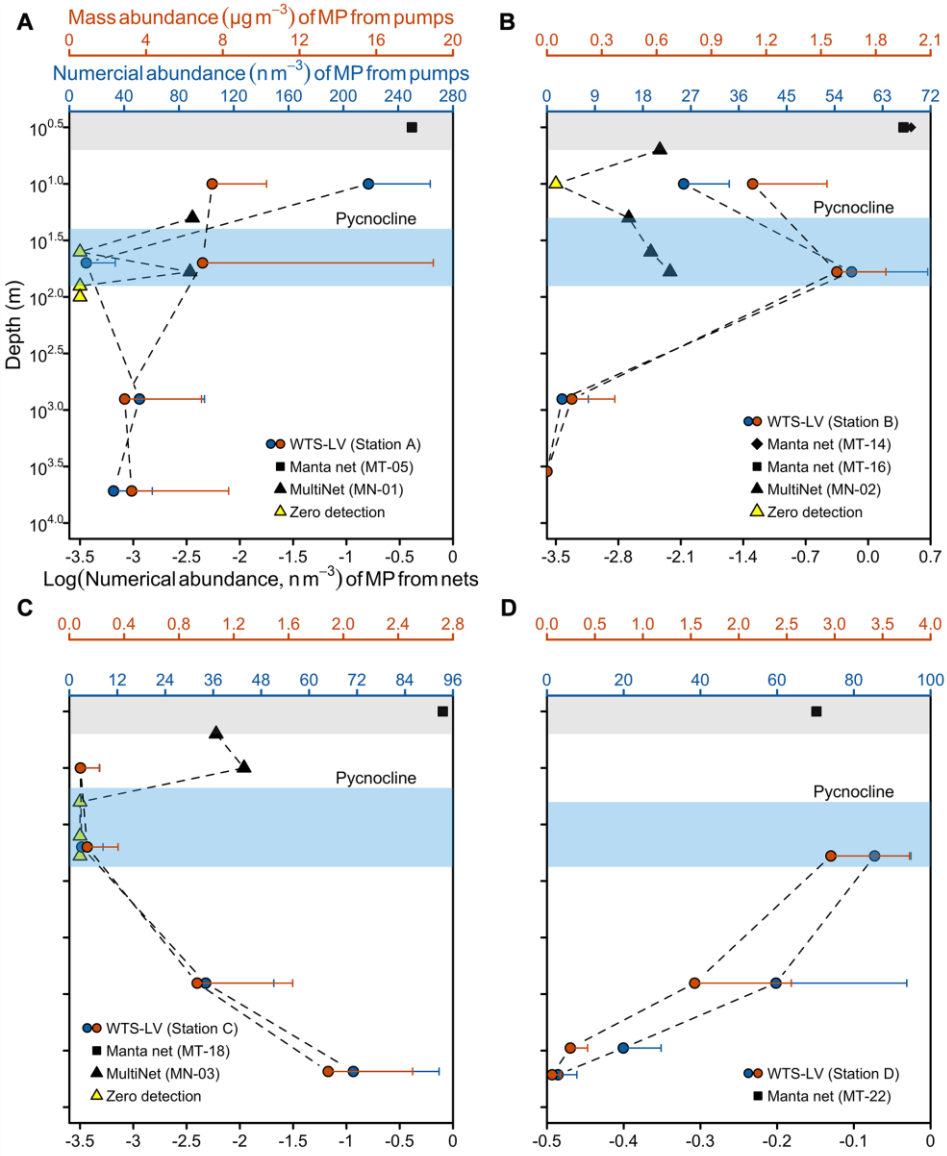

Fig. 2. Numerical, mass abundances of MP collected with the Manta net, MultiNet, and WTS-LV pump. (A) Station A, (B) Station B, (C) Station C, (D) Station D. The filled colors of points correspond to the respective x-axis. The values of the Manta net sample have been corrected for wind-induced mixing in the 5-m-thick ocean layer. The numerical abundances of plastics in the Manta net and MultiNet samples were log transformed. Yellow triangles represent the MultiNet samples in which no plastic fragments were found. Gray and light blue shades indicate the top 5 m of water column and approximate pycnocline layer, respectively. Error bars represent standard deviation.

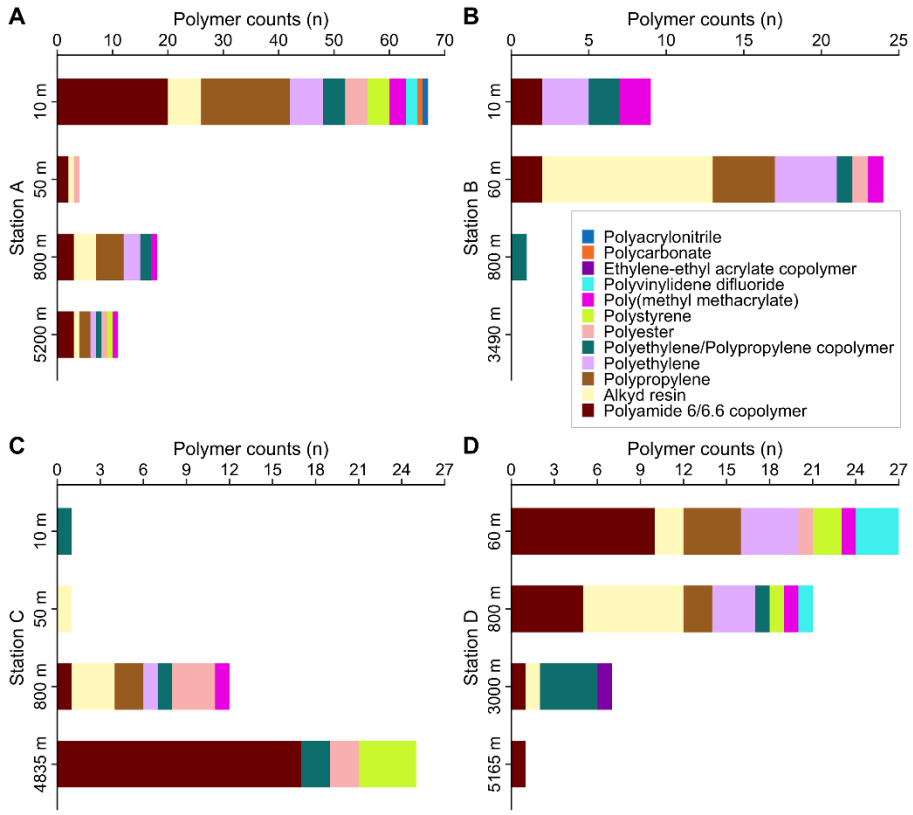

Fig. 3. Polymer composition profiles of SMP collected with WTS-LV pumps at four stations.

(A) Station A, (B) Station B, (C) Station C, (D) Station D.

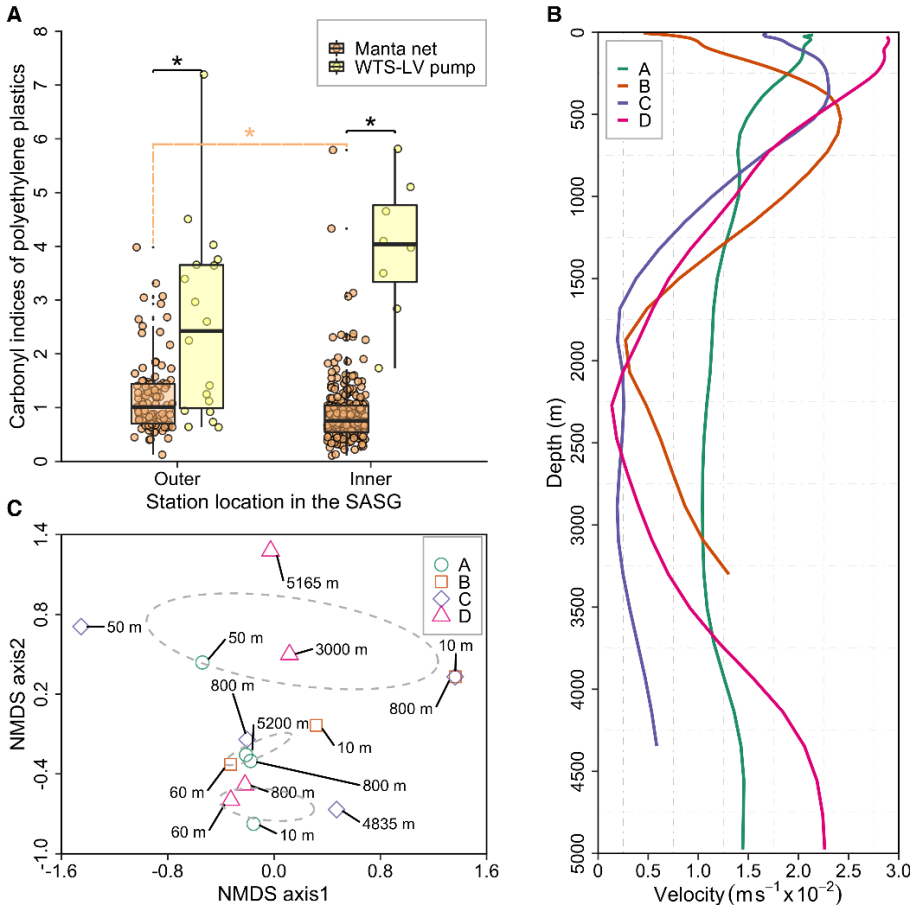

Fig. 4. (A) Carbonyl indices of polyethylene particles from the Manta net (orange boxplots) and WTS-LV pump (yellow boxplots) in the SASG. The "Outer" and "Inner" indicate the sampling regions located in the outer and inner accumulation zones of the SASG as shown in Fig. 1. Bold black horizontal lines represent boxplot medians; top and bottom of colored boxes represent 25th and 75th percentiles; and whiskers indicate the largest and the smallest measured values within 1.5 interquartile ranges from the box. Asterisks denote statistically significant differences between LMP and SMP (Mann-Whitney-Wilcoxon test, $p<0.05$). (B) The depth-dependent velocity profiles (m s^{-1} × 10^{-2}) at the four sampling stations averaged over 1993-2018. The dataset is from the Simple Ocean Data Assimilation reanalysis. (C) Non-metric multidimensional scaling (NMDS) ordination of polymer type composition identified in WTS-LV samples at each depth from all stations based on Bray-Curtis dissimilarities (Stress = 0.11). Ellipses in NMDS denote 95% confidence levels for the distinct clustering. Colored shapes represent four WTS-LV pump stations. The text labels indicate the sampling depth.

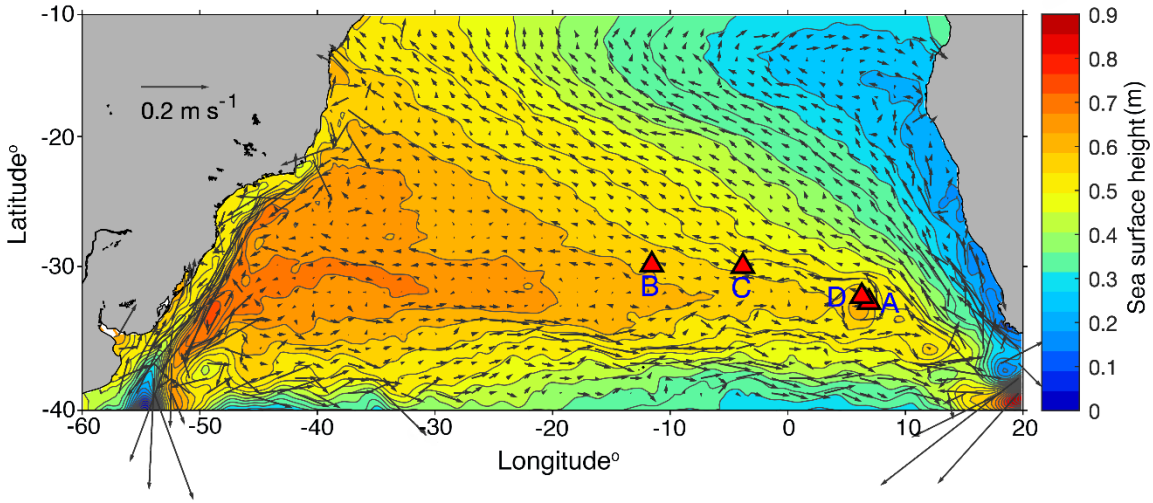

Fig. 5. Surface circulation in the South Atlantic. The mean sea surface height (m, color) with surface geostrophic velocities overlayed (m s^{-1}, vectors) over the South Atlantic during 1993-2018. The sampling locations are marked as red triangles. The dataset was obtained from the CMEMS.

Supplementary Materials

Supplementary Materials for

Large quantities of small microplastics permeate the surface ocean to abyssal depths in the South Atlantic Gyre

Shiye Zhao, Erik R. Zettler, Ryan P. Bos, Peigen Lin, Linda A. Amaral-Zettler, Tracy J. Mincer

*Corresponding authors: szhao@jamstec.go.jp, tmincer@fau.edu

This PDF file includes:
Figures S1 to S10
Tables S1 to S6
Reference 76-74

Other Supplementary Materials for this manuscript include the following:
Python code for polymer identification

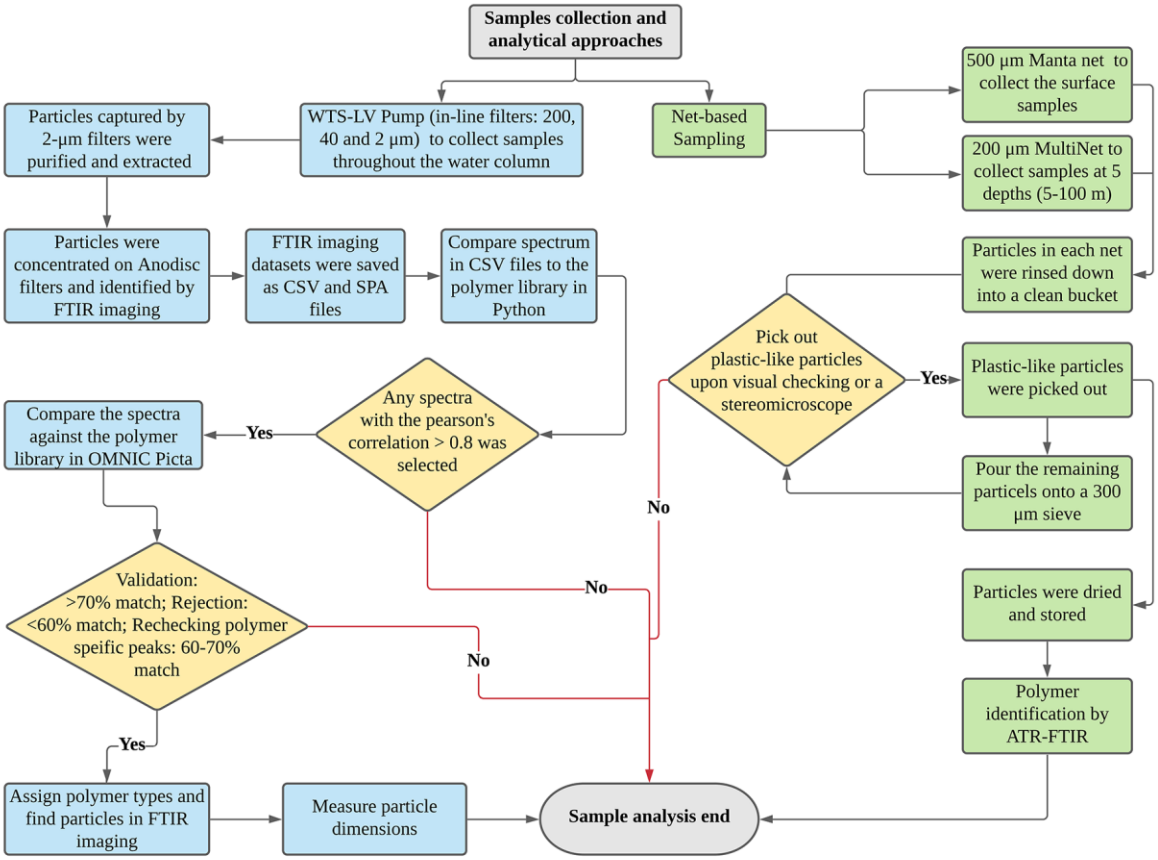

Fig. S1. The flowchart of samples collection and analysis in this study.

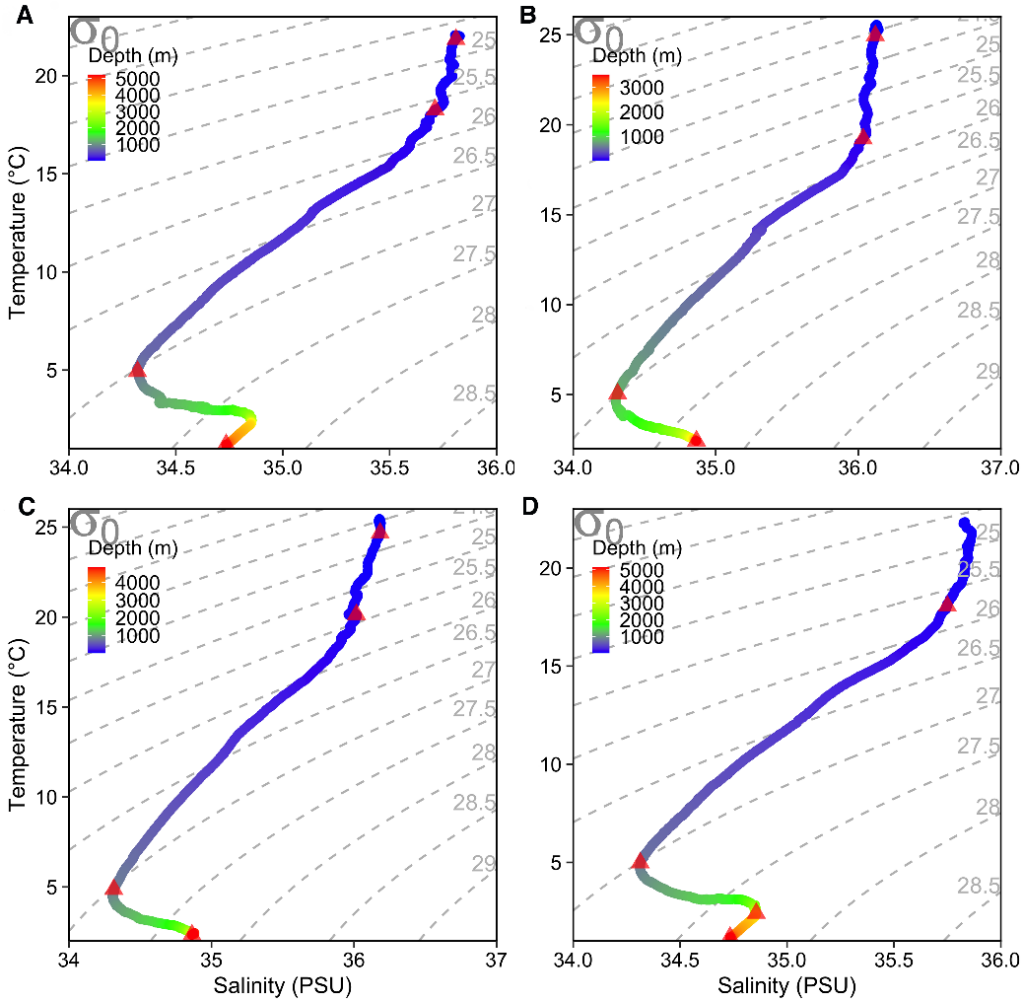

Fig. S2. Temperature-salinity diagram showing the presence of different water masses at four WTS-LV pump sampling stations in the SASG. (A) Station A, (B) Station B, (C) Station C, (D) Station D. The red triangles represent the depths where the pumps were deployed.

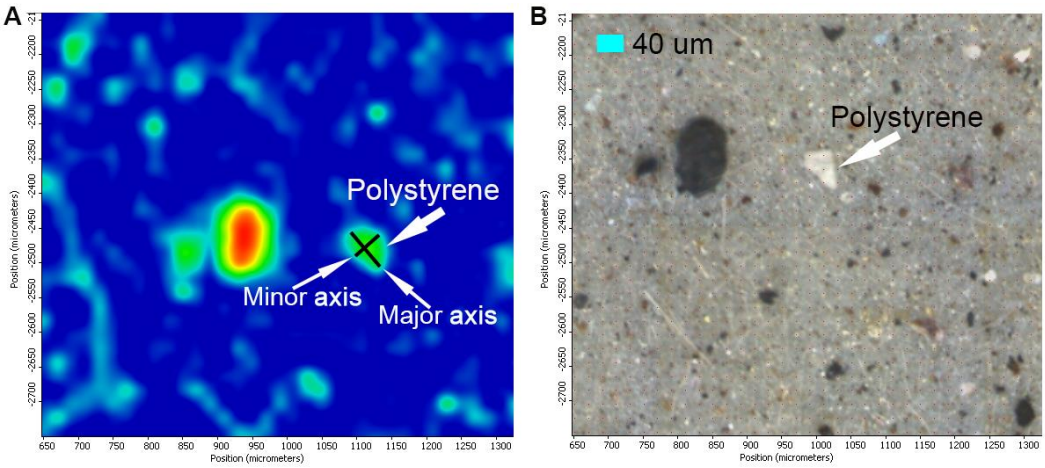

Fig. S3. The pseudo-color infrared imaging of a polystyrene (PS) particle highlighted in C–H stretch (A) and the optical image of this PS item (B). This particle was identified in the WTS-LV pump sample at 10 m depth, station A.

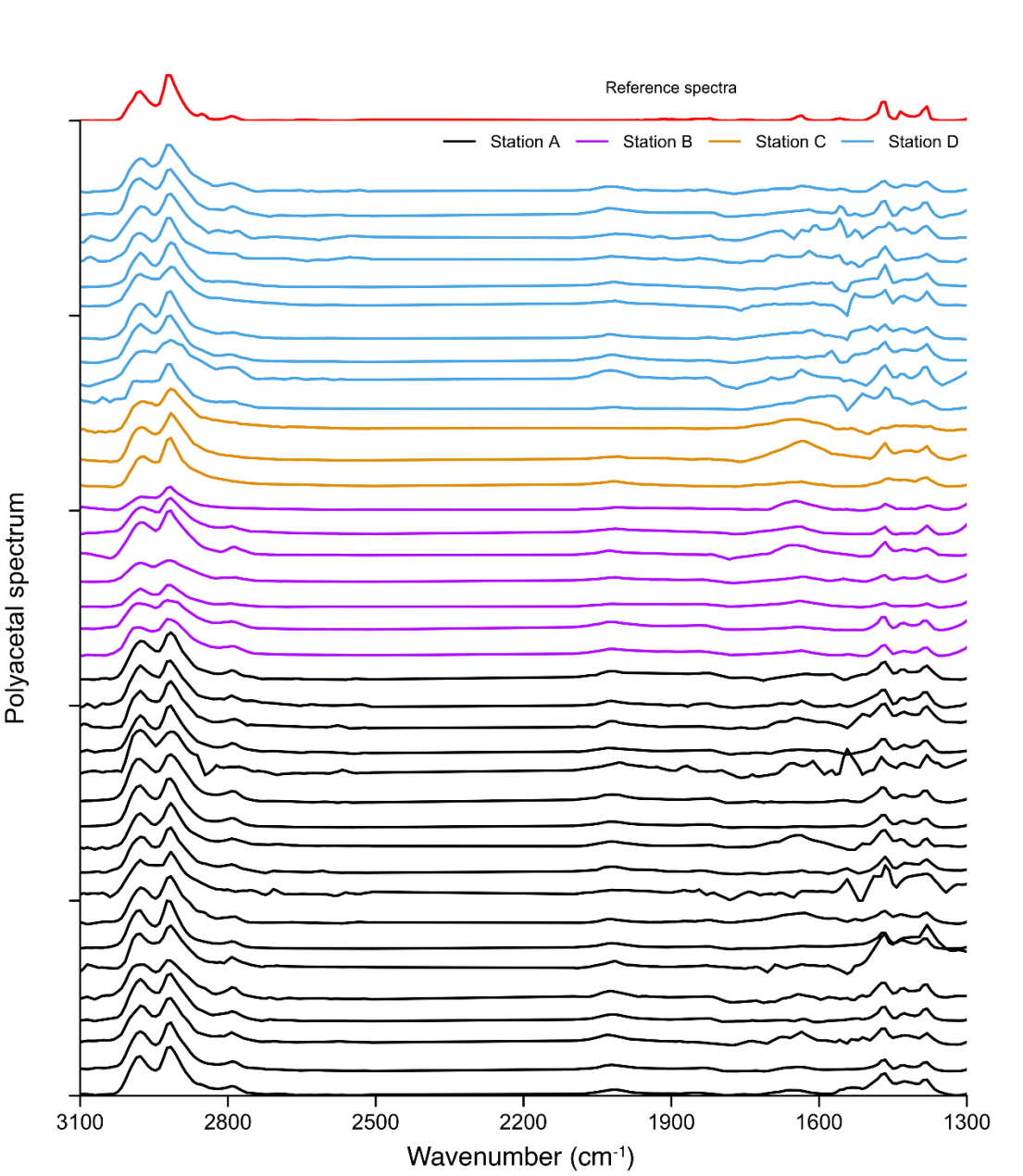

Fig. S4. FTIR Spectrum of Polyacetal particles (n = 38) detected in four stations. The reference spectrum (red) is from the library built by Primpke et al. (*4*).

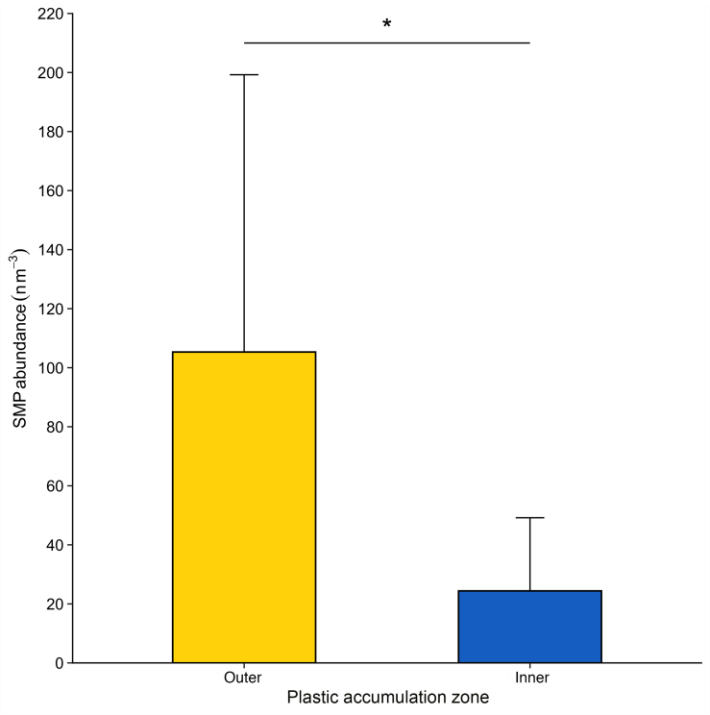

Fig. S5. Comparisons of SMP abundances at water depths <60 m in the outer accumulation zone of the SASG (Stations A and D) and the inner accumulation zone (Stations B and C). These are the abundances of pump samples collected in the top 60 m. Asterisk denotes statistically significant difference between two groups (Mann-Whitney-Wilcoxon test, $P < 0.05$).

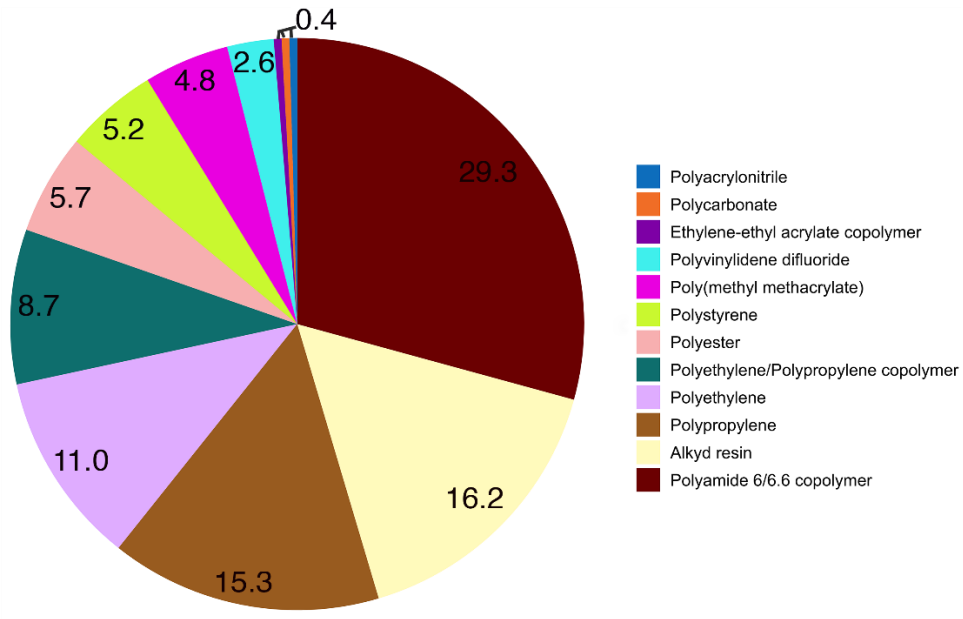

Fig. S6. Polymer composition (%) of all SMP particles identified in this study.

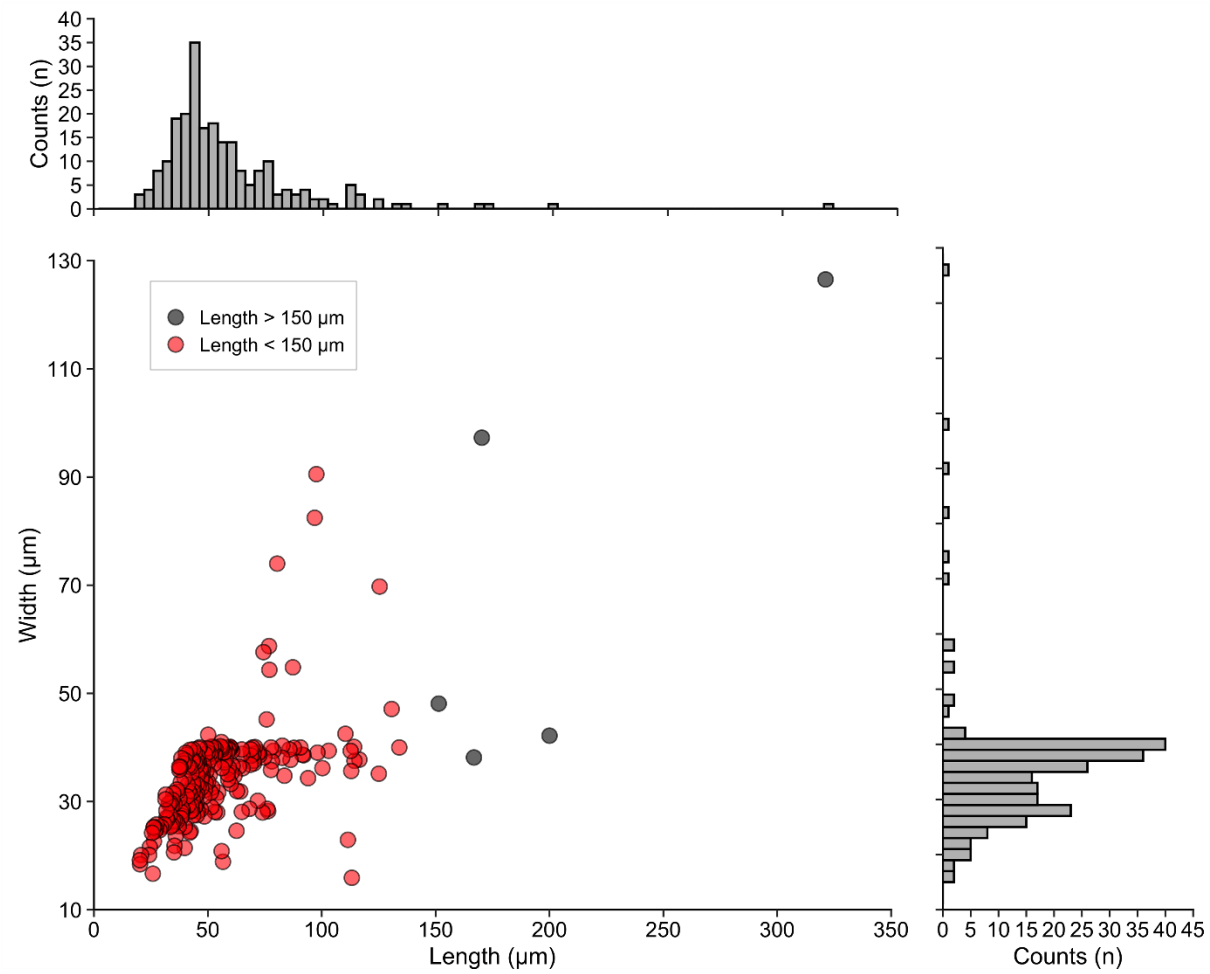

Fig. S7. Plastic size fractions of SMP collected by WTS-LV pumps at four stations. Red points represent the length of particles that are less than 150 µm, which is the upper size limit for particles translocating across the gut epithelium of animals (*19*).

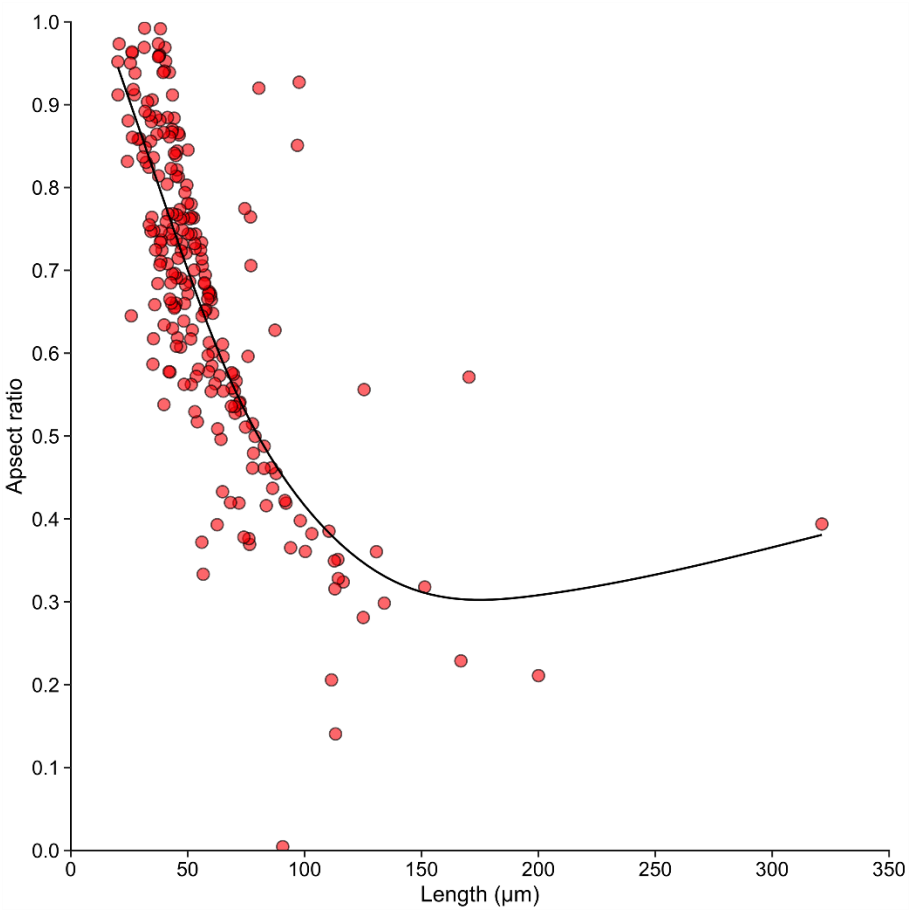

Fig. S8. Aspect ratio distribution of identified SMP as a function of particle length showing smaller particles approach a more spherical shape. Length is plotted on the x axis, and aspect ratio is plotted on the y axis. The fitted smooth regression with the Generalized Additive Modelling (R^2 = 0.63, P << 0.001, AIC = -332.2) is shown as a solid line.

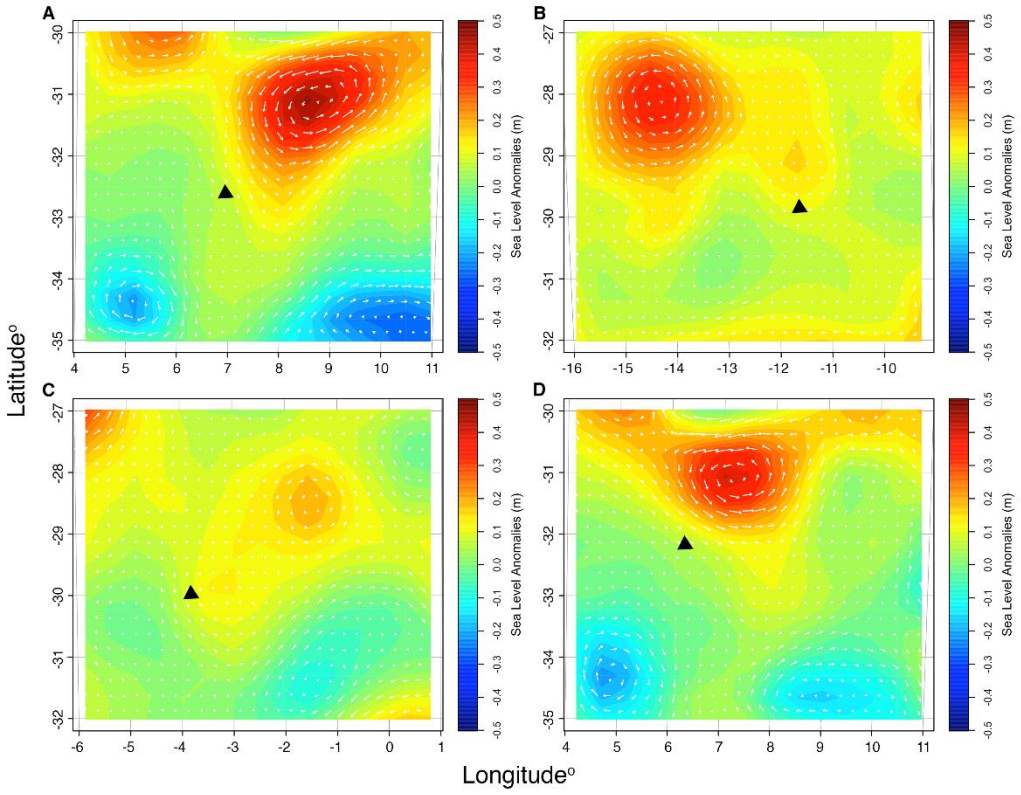

Fig. S9. Map of the sampled area within the South Atlantic Ocean correlated with Sea Level Anomalies satellite observations obtained from the CMEMS portal on the sampling days. (A) Station A, (B) Station B, (C) Station C, (D) Station D. The sampling site locations are marked as black triangles, showing stations A and D were closer to the core of the anticyclonic eddies. The vector denotes the sea surface geostrophic velocity anomaly (unit: m s^{-1}).

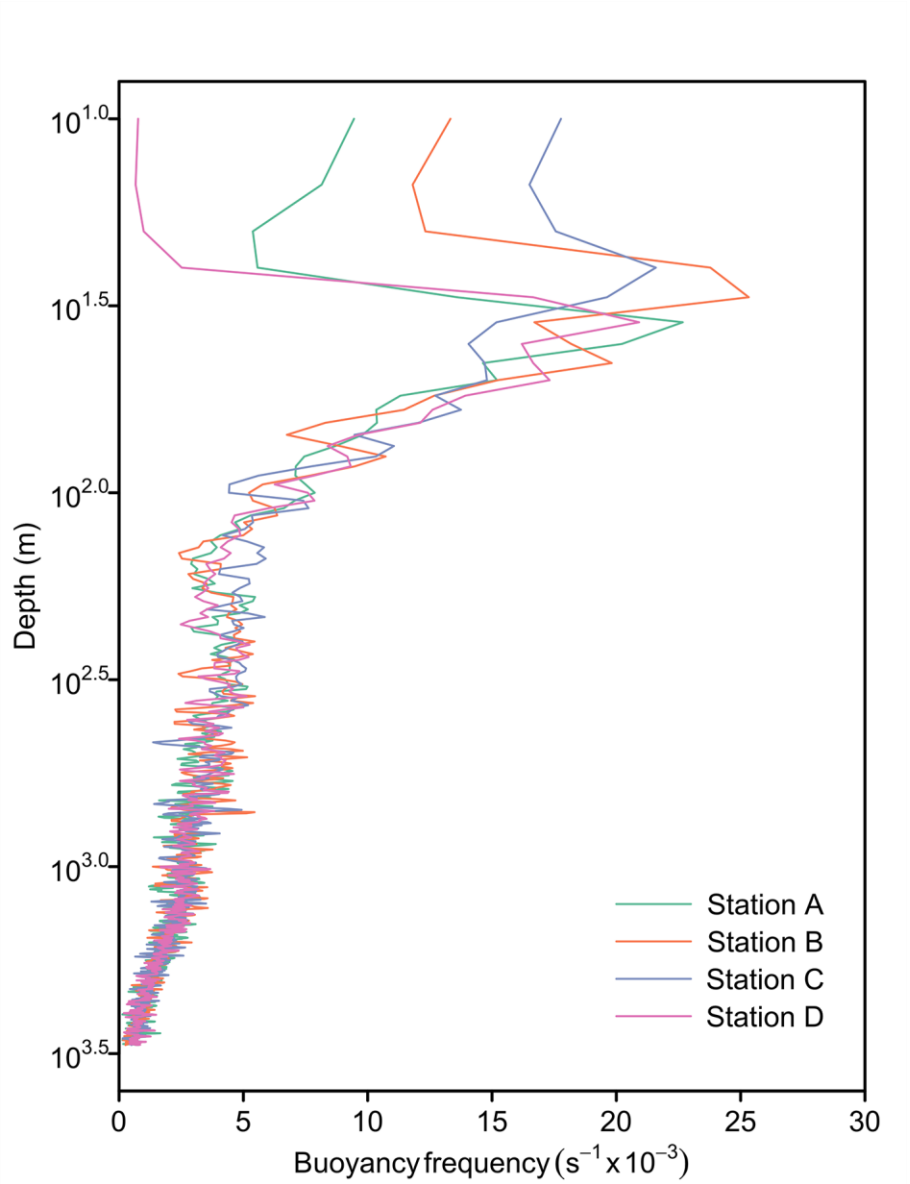

Fig. S10. The buoyancy frequency (s-1 × 10-3) at sampling stations.

Table S1. Details of the Manta net and MultiNet samplings.

Type	Date	Longitude /Latitude (start point)	Sites	Depth (m)	Filtering volume (m^3)	Plastic pieces (n)	Wind speed ($m\ s^{-1}$)	Abundance	
								($n\ m^{-3}$)	($\mu g\ m^{-3}$)
Manta net	7th Jan.	32.67°S/ 7.03°E	MT-05	0.15	185.74624	57	5.5	0.41	0.6×10^3
	13th Jan.	29.99°S/ 11.59°W	MT-14	0.15	236.12848	535	1.3	3.03	4.3×10^3
	15th Jan.	29.87°S/ 7.99°W	MT-16	0.15	280.69024	521	5.5	2.48	3.5×10^3
	16th Jan.	29.98°S/ 3.94°W	MT-18	0.15	310.75928	186	2.8	0.80	1.1×10^3
	20th Jan.	32.16°S/6.26°E	MT-22	0.15	202.186	107	1.6	0.71	1.0×10^3
MultiNet	7th Jan.	32.66°S/7.01°E	MN-01	20	557	2		3.6×10^{-3}	5.0
				40	652	0		0	0
				60	587	2		3.4×10^{-3}	4.8
				80	438	0		0	0
				100	665	0		0	0
	13th Jan.	29.97°S/11.59°W	MN-02	5	432	2		4.6×10^{-3}	6.5
				10	426	0		0	0
				20	482	1		2.1×10^{-3}	2.9
				40	546	2		3.6×10^{-3}	5.1
				60	665	4		6.0×10^{-3}	8.4
	16th Jan.	29.99°S/3.9°W	MN-03	5	501	3		6.0×10^{-3}	8.4
				10	457	5		1.1×10^{-2}	15.3
				20	390	0		0	
				40	447	0		0	
				60	562	0		0	

Note: Numerical and mass abundances of the Manta net sample in this table include correction by wind effect.

Table S2. The detailed information of WTS-LV samplings.

Station	Date	Start time (UTC)	Longitude /Latitude	Depth (m)	Filtering volume (L)	Water mass	Plastic pieces in subsamples (n)		
A	7th Jan.	31:03	32.60°S / 6.91°E	10	440	SACW	17	25	25
				50	1634	SACW	4	0	0
				800	1765	AAIW	1	5	12
				5200	1711	AABW	0	5	6
B	13th Jan.	21:20	29.88°S / 11.56°W	10	880	SACW	2	4	3
				60	1404	SACW	6	8	10
				800	1765	AAIW	0	1	0
				3490	1688	NADW	0	0	0
C	16th Jan.	21:27	29.99°S / 3.82°W	10	914	SACW	0	1	0
				50	1626	SACW	1	0	0
				800	1765	AAIW	6	2	4
				4835	1765	NADW	8	6	11
D	20th Jan.	10:00	32.17°S / 6.29°E	60	793	SACW	10	8	9
				800	1765	AAIW	11	3	7
				3000	1765	NADW	1	3	3
				5165	1759	AABW	0	0	1

Notes: SACW, South Atlantic Central Water; AAIW, Antarctic Intermediate Water; NADW, North Atlantic Deep Water; AABW, Antarctic Bottom Water.

Table S3. Polyacetal contaminants identified in samples from four WTS-LV pump vertical profiles.

Station	Depth (m)	Replicate #	Counts (n)
A	10	1	3
		2	9
		3	2
	50	1	1
		2	1
	800	3	1
	5200	3	1
B	10	2	4
		3	2
	60	1	1
C	800	1	1
		3	2
D	60	3	2
	800	1	2
		2	1
	3000	1	1
		2	4

Table S4. Statistical analysis of microplastic abundances in four vertical profiles.

Station	Statistical test	Depth	Abundance
			P-value
A	Kruskal-Wallis		0.04
	Mann-Whitney-Wilcoxon test	10 m vs 50 m	0.04
		10 m vs 800 m	0.04
		10 m vs 5200 m	0.04
		50 m vs 800 m	0.12
		50 m vs 5200 m	0.25
		800 m vs 5200 m	0.82
B	Kruskal-Wallis		0.02
	Mann-Whitney-Wilcoxon test	10 m vs 60 m	0.04
		10 m vs 800 m	0.04
		10 m vs 3490 m	0.03
		60 m vs 800 m	0.04
		60 m vs 3490 m	0.03
		800 m vs 3490 m	0.31
C	Kruskal-Wallis		0.02
	Mann-Whitney-Wilcoxon test	10 m vs 50 m	0.79
		10 m vs 800 m	0.04
		10 m vs 4835 m	0.04
		50 m vs 800 m	0.04
		50 m vs 4835 m	0.04
		800 m vs 4835 m	0.07
D	Kruskal-Wallis		0.03
	Mann-Whitney-Wilcoxon test	60 m vs 800 m	0.27
		60 m vs 3000 m	0.04
		60 m vs 5165 m	0.04
		800 m vs 3000 m	0.10
		800 m vs 5165 m	0.04
		3000 m vs 5165 m	0.12

Table S5. The theoretical density of polymer types identified.

Polymer type	Density (g cm^{-3})
Polypropylene	0.86
Ethylene-ethyl acrylate copolymer	0.93
Polyethylene	0.94
Polyethylene/polypropylene copolymer	0.95
Polystyrene	1.04
Polyamide 6/6.6 copolymer	1.14
Poly(methyl methacrylate)	1.18
Polyacrylonitrile	1.18
Polycarbonate	1.22
Polyester	1.39
Alkyd resin	1.6
Polyvinylidene fluoride	1.78

Notes: The density are sourced from the Polymer Database (CROW logo Polymer Science).

Table S6. Comparison of the settling velocities of marine particles in the current study (theoretical values) and in literature (measured values). ESD: equivalent sphere diameter.

Particles	Size (mm)	Sinking rate (10^{-3} × m s^{-1})	Reference
Microplastic	0.5-73	1.0-43.8	Reisser et al. (76)
Microplastic	0.3-3.6, ESD	6-91	Kowalski et al. (77)
Plastic debris	>0.5	25.0-249.6	Lebreton et al. (78)
Microplastic	0.63-3.48, ESD	5-105	Van Melkebeke et al. (79)
Faecal pellet (Copepod)	~0.45	1.0	Cole et al. (80)
Faecal pellet (Antarctic krill)	~0.5	2.0	Bergami et al. (81)
SMP	0.008-0.076, ESD	2.4 × 10^{-6}-1.0 × 10^{-3}	The current study

References

76. J. W. Reisser et al., The vertical distribution of buoyant plastics at sea: an observational study in the North Atlantic Gyre. *Biogeosciences* **12**, 1249-1256 (2015).

77. N. Kowalski, A. M. Reichardt, J. J. Waniek, Sinking rates of microplastics and potential implications of their alteration by physical, biological, and chemical factors. *Marine Pollution Bulletin* **109**, 310-319 (2016).

78. L. Lebreton et al., Evidence that the Great Pacific Garbage Patch is rapidly accumulating plastic. *Scientific Reports* **8**, 1-15 (2018).

79. M. Van Melkebeke, C. Janssen, S. De Meester, Characteristics and sinking behavior of typical microplastics including the potential effect of biofouling: implications for remediation. *Environmental Science & Technology* **54**, 8668-8680 (2020).

80. M. Cole et al., Microplastics alter the properties and sinking rates of zooplankton faecal pellets. *Environmental Science & Technology* **50**, 3239-3246 (2016).

81. E. Bergami, C. Manno, S. Cappello, M. Vannuccini, I. Corsi, Nanoplastics affect moulting and faecal pellet sinking in Antarctic krill (Euphausia superba) juveniles. *Environmental International* **143**, 105999 (2020).

Python code for polymer identification will be available on GitHub.